Emulsion-confined self-assembly of colloidal nanoparticles into 3D superstructures

Chaolumen Wu, Qingsong Fan, Yadong Yin*

SUMMARY

Organizing the colloidal particles into 3D superstructures is a promising strategy for fabricating functional metamaterials with novel optical, electric, and catalytic properties. The rich surface properties of the colloidal particles provide many ways to manipulate their assembly behavior. Emulsion droplets are ideal microspaces for confining colloidal self-assembly, offering many advantages such as versatility, scalability, and controllability over size, shape, and composition. In this review, we first introduce recently developed strategies for the emulsion-confined assembly of colloidal particles into 3D superstructures by manipulating the interfacial properties of the emulsion droplets and colloidal particles, then demonstrate the novel collective properties of the assembled superstructures and highlight some of their unique optical and catalytic properties and applications in bioimaging, diagnosis, drug delivery, and therapy.

INTRODUCTION

An emulsion is a dispersion of two normally immiscible liquids in which one phase (dispersed phase) is present in the form of droplets in the other (continuous phase).[1-4] Surfactants are typically used to stabilize the droplets temporarily by reducing the interfacial tension. Emulsions have widespread applications in our daily lives, such as in food, cosmetics, petroleum, pulp and paper, and the agricultural and pharmaceutical industries.[5-7] The droplet form and the unique surface properties of the emulsions also offer an elegant pathway to synthesize polymer particles through a process defined as emulsion polymerization, producing waterborne resins with diverse colloidal and physicochemical properties.[8-11]

Depending on the nature of the dispersed phase, emulsions can be classified into four different types (as shown in Scheme 1): water-in-oil (W/O), oil-in-water (O/W), water-in-oil-in-water (W/O/W), and oil-in-water-in-oil (O/W/O).[2,4,12] Within them, W/O and O/W are the most common emulsions, and their detailed structures are shown in Scheme 1. For

O/W emulsion, the hydrophobic heads of surfactants contact oil (dispersed phase), and the hydrophilic tails contact water (continuous phase) to stabilize the droplets, while the situation is reversed for W/O emulsion.[4] According to their droplet sizes, the emulsion family is generally divided into macroemulsion and miniemulsion, with the former ranging from 1 μm to 100 μm and the latter from 50 nm to 1 μm.[13]

Inherently, emulsions are thermodynamically unstable due to the great surface tension between oil and water.[2,12] Thus, adding surfactants is a prerequisite for forming kinetically stable emulsions. The stability of the emulsions can be expressed by the interfacial force that can be characterized by the Laplace pressure (ΔP_L), as shown in the following equation:

$$\Delta P_L = \frac{2\gamma}{r}$$

where γ is the interfacial tension between oil and water, and r is the emulsion droplet radius.[2] The presence of the surfactant can greatly decrease the interfacial tension, resulting in decreased interfacial force and a longer lifetime of emulsions. Typically, emulsions are stabilized by the electrostatic or steric repulsion from the surfactants. The absorption of the ionic surfactants can induce the electrical double layers around the emulsion droplet, preventing droplet contact. Nonionic surfactants and polymers can prevent the close contact of droplets by the steric effect.[2,12]

The kinetic stability of the emulsions, especially macroemulsion, enables their function as soft templates to confine the well-dispersed nanoparticles within the droplets and assemble them into superstructures.[14-16] With surfactants, the emulsions can be stable during assembly, even under relatively high-temperature evaporation, producing well-defined superstructures. Besides the small-molecule surfactants and polymers, colloidal particles can also serve as stabilizing agents to form Pickering emulsions.[17-19] The particles at the oil-water interface can greatly decrease the surface tension and produce structures featuring a hollow space, large surface area, low density, and abundant active sizes, promising for applications such as drug delivery, controlled release, and catalysis.[20,21]

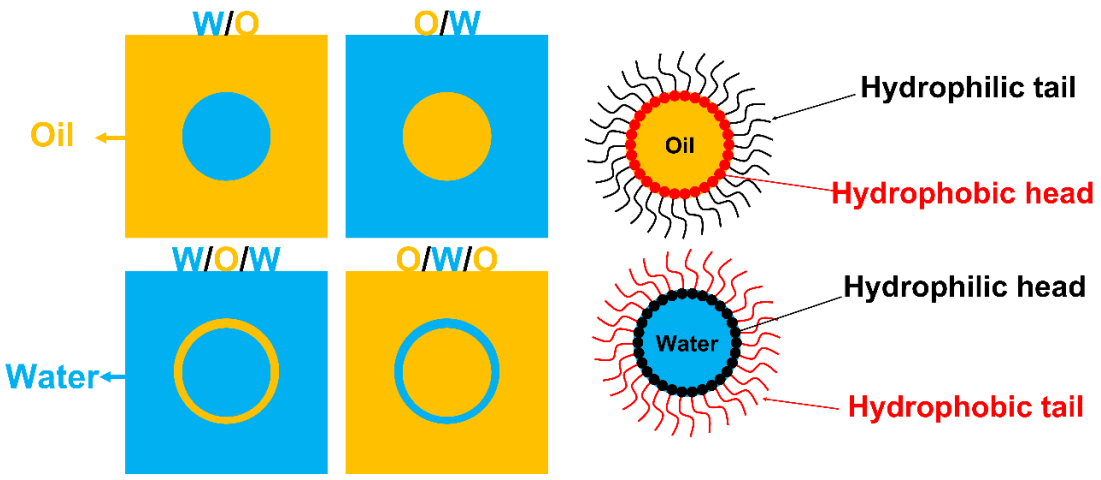

Scheme 1. Classification of emulsions by the nature of the dispersed phase.

Colloidal nanoparticles with a narrow size distribution, well-protected surfaces, uniform shapes, and tunable properties can be easily synthesized by many synthesis methods, such as thermolytic and hydrothermal reactions.[22-27] Emulsion-confinement provides a general way to self-assemble these colloidal nanoparticles into superstructures with good stability, tunable sizes, shapes, and compositions, and collective electronic, magnetic, and optical properties, which are highly desirable for many important applications in the fields of catalysis, optical devices, biological labeling and imaging, and disease treatments.[14,28-35]

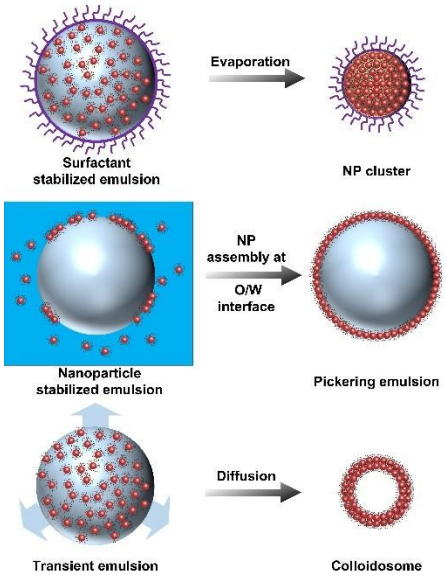

Scheme 2. Schematic illustration of three different types of emulsion-confined self-assembly processes.

In this review, we aim to discuss the emulsion-confined self-assembly of colloidal particles into 3D superstructures from the perspective of emulsion surface properties and summarize the currently developed emulsion-confined assembly methods. We start with a general introduction to the working principle of emulsion-confined self-assembly, then discuss three methods based on different surface stabilizing agents, namely, surfactant-stabilized emulsions, nanoparticle-stabilized Pickering emulsions, and surfactant-free transient emulsions (as shown in Scheme 2). A detailed discussion is made on how these different strategies contribute to the different assembly behaviors of nanoparticles and the assembled superstructures (as shown in Table 1). We highlight some unique optical and catalytic properties and biomedical applications of the superstructures. (as shown in Table 1) Lastly, we conclude with the current progress and our perspectives on the challenges and future directions of the emulsion-confined self-assemblies.

Table 1. Summary of three different emulsion-confined assembly systems

Type	Stabilizer	Stability	Building blocks	Applications
Surfactant-stabilized emulsion	surfactant (small molecules/ polymers)	kinetically stable	molecules, polymers, nanoparticles	bioimaging, therapy, catalysis, optical devices
Nanoparticle-stabilized emulsion	nanoparticles	kinetically stable	nanoparticles (>50 nm)	drug delivery, catalysis
Transient emulsion	no	unstable	ions, biomolecules, nanoparticles	light absorbers

EMULSION-CONFINED SELF-ASSEMBLY

Typical emulsion-confined self-assembly involves first emulsification of the oil phase containing colloidal nanoparticles with water phase containing surfactants into O/W emulsion droplets or micelles, and then the aggregation of the nanoparticles induced by solvent evaporation or demulsification (as shown in Scheme 3).[14,16,36] The formation of emulsion droplets or micelles depends on the concentration of the surfactants. If the value

is higher than critical micelle concentration (CMC), there are enough surfactants to stabilize each nanoparticle to form micelles. If the value is lower than the CMC, macroemulsion droplets form, encapsulating many nanoparticles in each droplet. The final assembled structures are protected by a layer of surfactants thanks to the Van der Waals interaction between the hydrophobic capping ligands on the nanoparticle surface and the hydrophobic tails of the surfactants, enabling good dispersibility in water.[14]

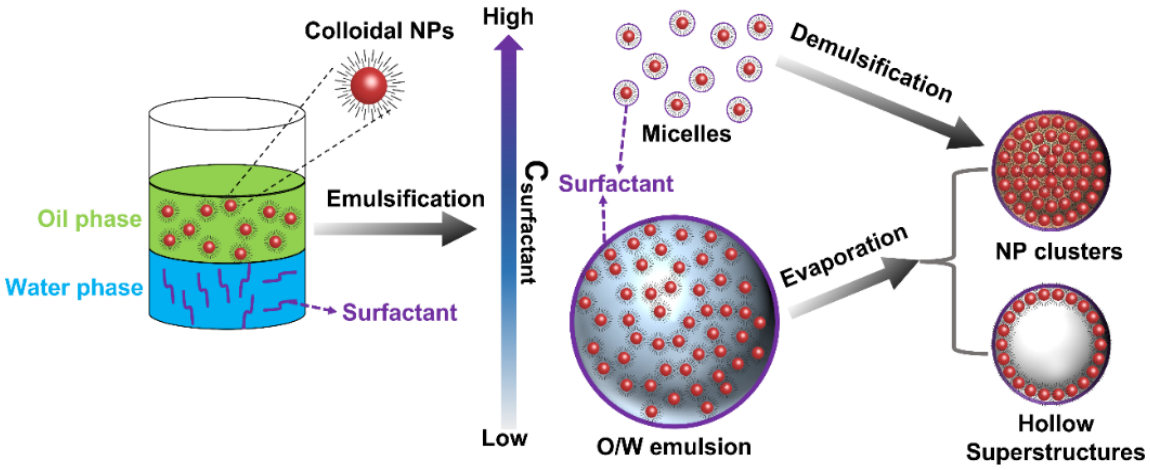

Scheme 3. Schematic illustration of the emulsion-confined self-assembly of colloidal nanoparticles into 3D superstructures.

Besides typical surfactants like small-molecule surfactants or polymers, nanoparticles can also serve as stabilizing agents and attach to the interface of water and oil to form colloidosomes.[21,37-39] Furthermore, researchers recently have developed surfactant and nanoparticle co-stabilized emulsion-confined assembly[40,41] and surfactant-free transient emulsion-confined assembly to fabricate superstructures with smaller sizes and different morphologies.[42,43] Therefore, in the following sections, we discuss the assembly mechanisms and resulting superstructures of four emulsion-confined assembly methods based on micelles, surfactant stabilized emulsions, nanoparticle-stabilized Pickering emulsions, and surfactant-free transient emulsions.

Micelle-based self-assembly

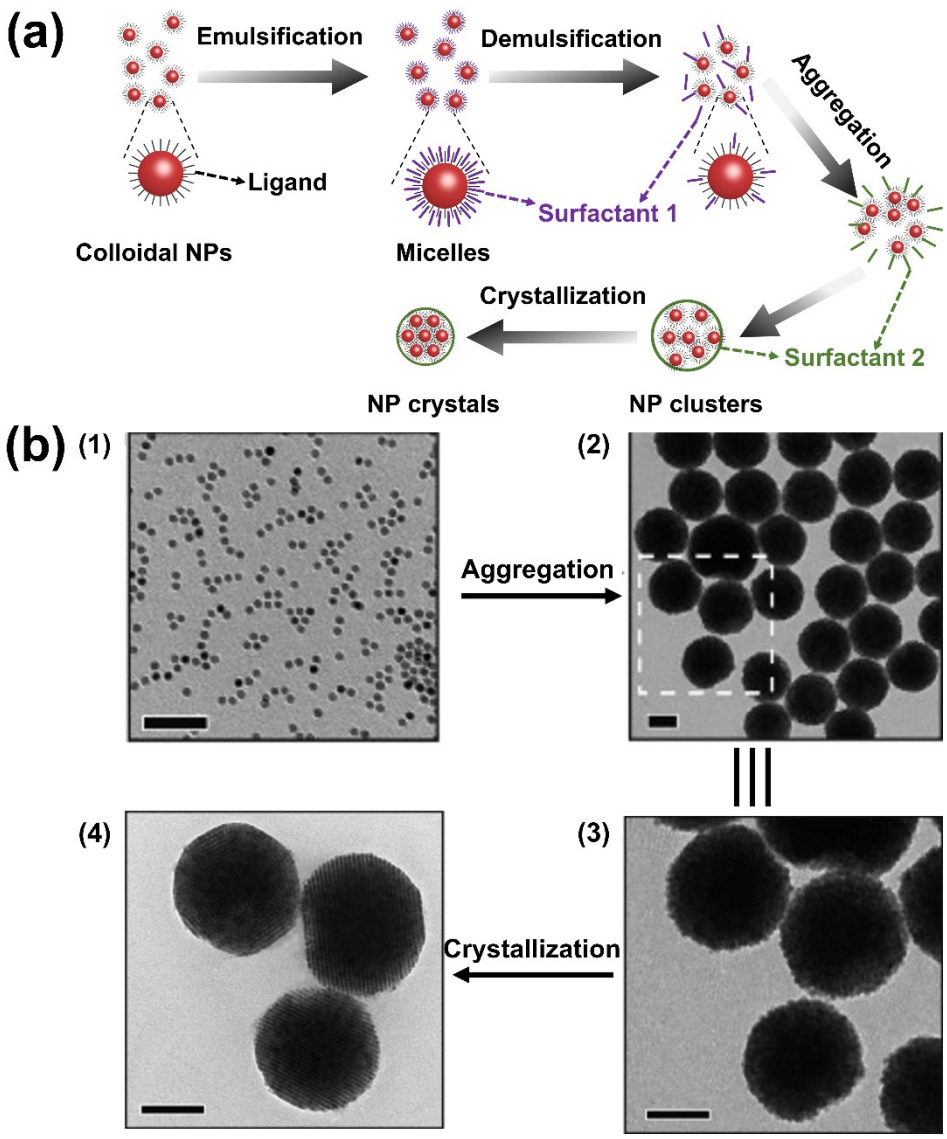

Figure 1. Micelle-based self-assembly of colloidal nanoparticles into close-packed 3D superstructures. (a) Scheme of the proposed assembly mechanism of 3D superstructures. (b) TEM images of the DTAB Fe_3O_4 micelles and the assembled structures with the addition of PVP and final 3D superstructures after crystallization.[44]

When the concentration of surfactants is higher than CMC, each colloidal nanoparticle can be coated by a layer of surfactants, producing water-dispersible micelles. Subsequent demulsification can destabilize the micelles, inducing nanoparticle aggregation into clusters (Figure 1a). For example, Cao et al. utilized solvophobic interactions to remove the surfactant from the micelles and promote the aggregation of Fe_3O_4 nanoparticles into

superparticles.[36,44] The dodecyltrimethylammonium bromide (DTAB) stabilized micelles were demulsified due to the solvophobic interactions between ligands on the nanoparticle surface and the solvent ethylene glycol (process (1) to (2) in Figure 1b). Poly(vinylpyrrolidone) (PVP) was added during the assembly to stabilize the resulting nanoparticle clusters, providing them with good dispersibility. This rapid process could assemble nearly all the nanoparticles into clusters within 1 min, producing amorphous superparticles, which could be converted into single crystals by further annealing (process (4) to (5) in Figure 1b). The final superparticles adopted a near-spherical shape to minimize the surface energy. The size of the superparticles could be easily controlled by tuning the molar ratio between DTAB and Fe_3O_4 nanoparticles, with a smaller ratio producing larger superparticles. In addition, the morphology of the superparticles is found to be related to the shape of the original building blocks. When nanocubes were used as building blocks, they could be assembled into superparticles with a cubic shape by introducing a small amount of oleic acid into the superparticle growth solution to precisely control the particle interactions. The increased oleate ligands on nanocubes resulted in the increased van der Waals interactions between nanocubes, which decreased the surface tension and adopted a cubic shape to decrease the overall Gibbs free energy.[45] This micelle-based method has also been used to self-assemble nanorods into superparticles with multiple crystal domains, and the morphology could be controlled to produce single-domain, needle-like superparticles by introducing anisotropic interactions between nanorods.[46] When two different nanoparticles were employed as building blocks, they could be co-assembled into core-shell superstructures, as demonstrated in the example of co-assembling Fe_3O_4 nanoparticles and CdSe-CdS core-shell quantum dots (QDs) into superstructures each composed of a Fe_3O_4 core and a QD shell.[47] The micelle-based assembly represents a versatile approach to organizing colloidal nanoparticles into superstructures with tunable sizes and shapes.

Surfactant-stabilized emulsion-confined self-assembly

Macroemulsion droplets encapsulating colloidal nanoparticles are formed from the emulsification of the water and oil phase when the surfactant concentration is lower than the CMC. They are kinetically stable and can serve as soft templates for nanoparticle

assembly.[16,48-51] As shown in Figure 2a, after the formation of emulsions, the assembly is initiated by the evaporation of low-boiling-point solvent within droplets. The nanoparticle concentration keeps increasing with the evaporation, and when the volume fraction of colloidal nanoparticles increases to ~20%,[52] nanoparticles start interacting with each other through hydrophobic-hydrophobic interactions, forming aggregates and finally nanoparticle clusters. As shown in Figure 2b, Li et al. reported the assembly of nanocrystals with different sizes, shapes, and components into 3D spherical structures by encapsulating them within macroemulsion droplets and then subsequent evaporation.[16] Figure 2b shows an example where $BaCrO_4$ or Ag_2S nanocrystals were assembled into 3D colloidal spheres with sizes of 100-120 nm and good dispersity in water due to the surface-attached surfactants. These colloidal spheres can further serve as building blocks to assemble into 2D arrays on a TEM grid, promising for fabricating more complex macroscopic functional architectures.[53,54] Moreover, the superstructures assembled from magnetic nanoparticles can be further assembled into 1D photonic crystals under external magnetic fields, exhibiting dynamically tunable photonic bandgaps.[55,56] Besides spherical nanocrystals, nanocubes,[57] nanoplates,[16] and nanorods[50,51] can also be assembled into 3D colloidal spheres. The size of the assembled structures can be fine-tuned by controlling the nanocrystal concentration, surfactant concentration, emulsification process, and oil-to-water ratio. Furthermore, facile control of the surface charges of the assembled structures can be achieved by employing various types of stabilizing agents, including anionic (e.g., sodium dodecyl sulfate), cationic (e.g., cetyltrimethylammonium bromide), and nonionic (e.g., P123) surfactants.[16]

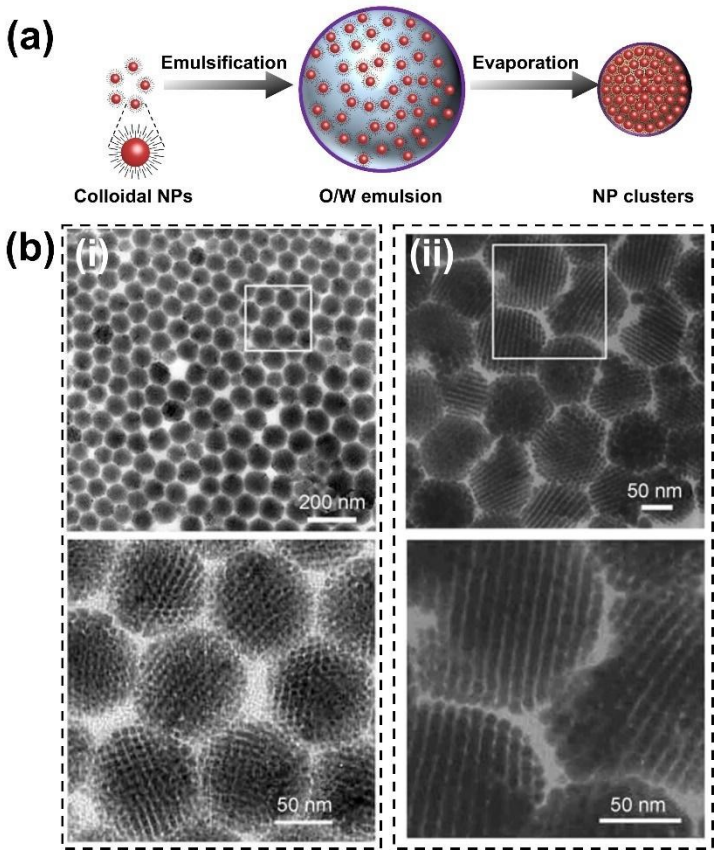

Figure 2. (a) Schematic illustration of the emulsion-confined assembly of colloidal nanoparticles into close-packed 3D superstructures. (b) Typical TEM images of superstructures assembled from the $BaCrO_4$ (i) and Ag_2S (ii) colloidal nanocrystals.[16]

The ordering and morphology of the superstructures can be precisely controlled by the assembly conditions and emulsion surface properties. The evaporation rate of the oil phase is one of the important factors that can greatly affect the order of the assembled structures.[58,59] As shown in Figure 3a, the assembled structures show good order at an evaporation temperature of 20 ℃, while a gradual transition from crystalline to amorphous occurs with increasing the evaporation temperature to 40, 60, and 80 ℃.[59] The decreasing drying time at higher temperatures inhibits the assembled structures from reaching their thermodynamically stable configuration. On the other hand, Wang et al. reported that a higher evaporation temperature led to improved crystallinity. In their case, it is believed that the high thermal energy under high temperatures facilitates the adjustment of nanoparticle position and counteracting the configurational entropy loss.[60] In addition, the crystallinity of the assemblies also depends on the emulsion properties, such as the

interfacial tension and choice of oil phase solvent. The crystallinity of the assembled structures greatly increases at increasing surfactant concentration while leaving the crystalline structures and volume fraction unchanged. The increased surfactant concentration further decreases the interfacial tension, resulting in a more deformable liquid-liquid interface to accommodate the positional optimization. The choice of solvent for the oil phase also affects the crystallinity of the assembled superstructures, with high-boiling-point oil generally yielding better crystallinity due to the lower evaporation rate. For example, using pentane as an oil phase resulted in amorphous assemblies, while switching to hexane significantly enhanced the crystallinity. Even higher crystallinity could be obtained using cyclohexane or chloroform as the oil phase. On the other hand, the interfacial tension must also be considered when choosing different solvents for the oil phase. For example, the boiling point of chloroform is lower than cyclohexane, while the former yields more ordered superstructures than the latter due to the lower interfacial tension between chloroform and water.[59] In addition, the dispersibility of colloidal nanoparticles in the oil phase also affects the crystallinity of the superstructures. A good solvent can ensure the free movement of the colloidal nanoparticles during evaporation, yielding assemblies with good crystallinity. In contrast, a poor solvent induces the aggregation of the colloidal nanoparticles in the early evaporation stage, resulting in amorphous superstructures.[61]

In addition to 3D close-packing, nanoparticles may also be assembled into hollow superstructures by choosing a proper solvent and evaporation temperature.[62] As shown in Figure 3b, when chloroform was used as an oil phase solvent, solid spherical structures were formed by evaporation at 80 ℃. In contrast, hollow structures were formed when the evaporation temperature was 40 ℃, primarily attributed to the partial solubility of chloroform in water. Under low evaporation, chloroform diffuses out, and water diffuses into the oil droplets, resulting in the accumulation of hydrophobic nanoparticles between the water-oil-water interface, and finally, the formation of hollow structures after the complete evaporation of chloroform.

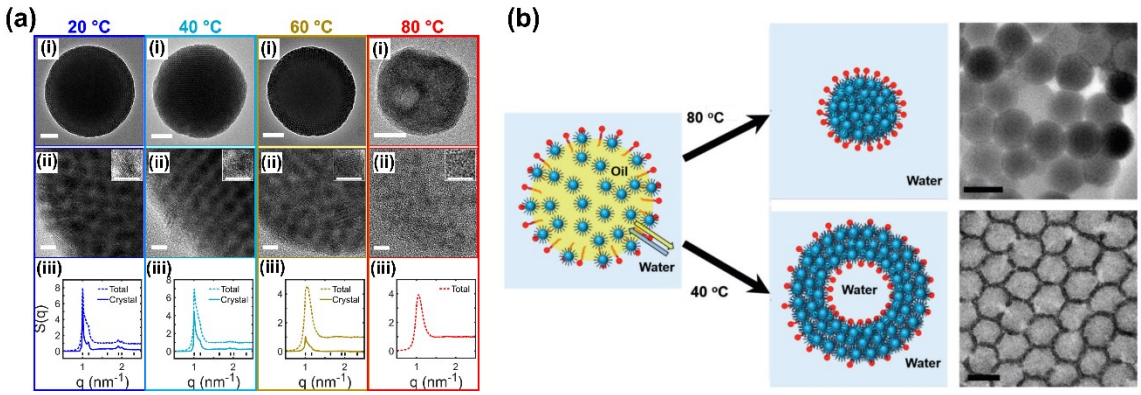

Figure 3. Evaporation temperature affects the crystallinity and morphology of the assembled structures. (a) Intermediate (i) and high (ii) resolution TEM micrographs of CdSe nanoparticles superstructures assembled from an emulsion dried at the indicated temperatures. Scale bars: 50 nm (i) and 5 nm (ii). (iii) The corresponding SAXS spectra of the assembled superstructures.[59] (b) Schematical illustration and TEM images of the assembled structures from iron oxide nanoparticles encapsulated in chloroform-water emulsions under different evaporation temperatures.[62]

As a general approach, the emulsion-confined assembly can be extended to fabricate more complicated functional superstructures by co-assembling two types of nanoparticles. In the past decades, many binary superstructures were fabricated from different building blocks such as Au/Fe_3O_4,[63-65] QDs/Fe_3O_4,[47] LaF_3:Eu/LaF_3:Yb-Er,[66] $CoFe_2O_4$-Fe_3O_4,[67] PbSe/CdSe,[68] and Au/QDs,[69] showing synergetic optical, magnetic, and catalytic properties. The binary assemblies can be superlattices,[67] core-shell,[47] Janus,[70] or amorphous structures,[69] depending on the size, number ratio, surface property of the building blocks, and also assembly conditions like surfactant and pressure.[71] In 2016, Kister et al. systematically studied the formation mechanisms of the crystalline, Janus, and core-shell binary superstructures, as shown in Figure 4.[70] The formation of the superstructures is dominated by nucleation, and earlier nucleation produces AB_{13} superlattice (Figure 4a, b(i)), while later nucleation produces core-shell (Figure 4a, b(iii)) or Janus structures (Figure 4a, b(ii)). Experimentally, the nucleation can be controlled by the size of the nanoparticles and the length of the surface ligands. Larger nanoparticles nucleate earlier than small ones due to the stronger attraction, while shorter ligands induce earlier nucleation due to less repulsion. Figure 4a(iv) shows the assembly process of the

Janus superstructures: the larger nanoparticles aggregate in an early stage and form clusters, while smaller ones aggregate later, forming the Janus structure. Since pressure affects the dispersibility of the nanoparticles, a higher pressure induces later nucleation, forming Janus or core-shell structures.

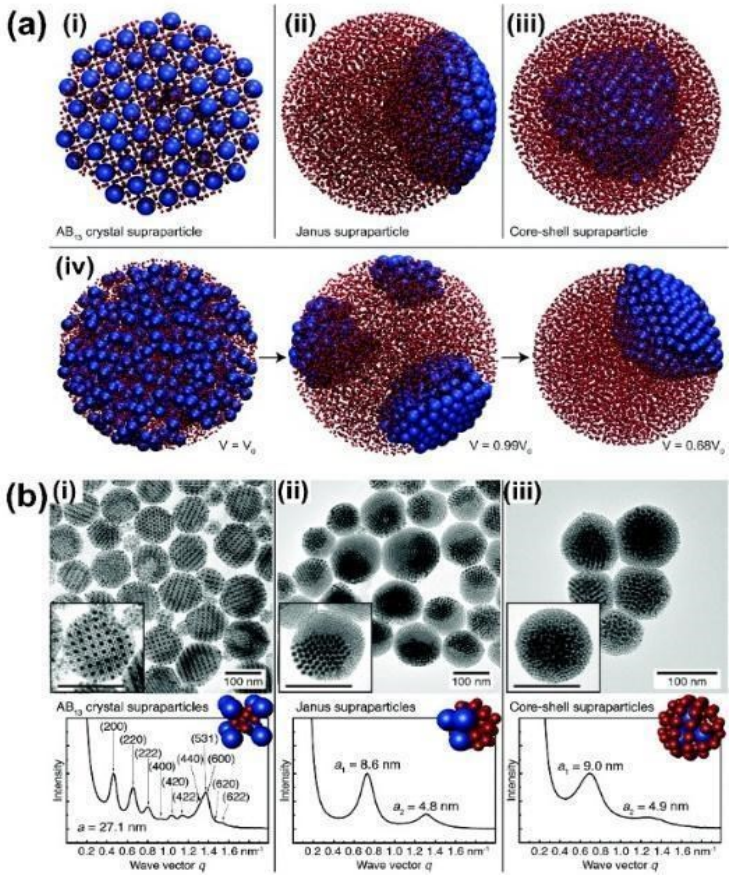

Figure 4. Controlling the assembled structures of binary superparticles. (a) Molecular dynamic simulations of nanoparticles confined in a spherical container that shrank during the simulation, (i) AB_{13} lattice, (ii) Janus structure, and (iii) core-shell structure; (iv) Snapshots of the formation of a Janus supraparticle in a shrinking container. (b) TEM and small-angle X-ray scattering (SAXS) of different assembled structures from the gold nanoparticle with diameters of 4 and 8 n in a concentration ratio of 13:1: (i) AB_{13} lattice, (ii) Janus structure, and (iii) core-shell structure.[70]

Binary supercrystals with tunable structural lattices can be achieved by controlling the surface property, size, and concentration ratio of two types of nanoparticles.[72-74] Within them, the ratio of two building blocks is a critical factor affecting the phase diagram of the

binary structures.[75-77] To study the concentration ratio effect separately, Wang et al. used 10-nm Fe_3O_4 and-5 nm Au nanoparticles as building blocks and assembled them into binary supercrystals of different lattices (as shown in Figure 5a).[64] The post-treatment of both nanoparticles with long-chain alkyl molecules (e.g., oleic acid) is crucial to forming supercrystals since different nanoparticles usually possess completely different surface chemistry and interactions. When the concertation ratio of Au and Fe_3O_4 nanoparticles is around 15:1, an ico-$NaZn_{13}$-type lattice is formed, as shown in Figure 5b-e. When the ratio is decreased to around 1:10, larger Fe_3O_4 nanoparticles assemble into an ordered FCC lattice, with smaller Au nanoparticles acting as "dopants". When the concentration of Au nanoparticles gradually increases, other types of lattices like AlB_2 and $AuCu_3$ are formed. Even more complicated binary supercrystal structures can be formed by controlling the size and the number ratio of two building blocks.[67] For example, Fe_3O_4 nanocrystals with diameters of 8.5 nm and 17 nm can assemble into AB_{13}-type binary supercrystals when the number ratio of small to large nanocrystals is around 13:1. However, disordered superparticles are formed when the particle number ratio is lower than 13:1, while core-shell superparticles featuring AB_{13}-type binary supercrystals cores and small nanocrystal shells are formed when particle number ratio is larger than 13:1. Furthermore, $MgZn_2$, NaCl, and $CaCu_5$ binary supercrystals have also been realized by choosing the proper size and number ratio of the two building blocks.

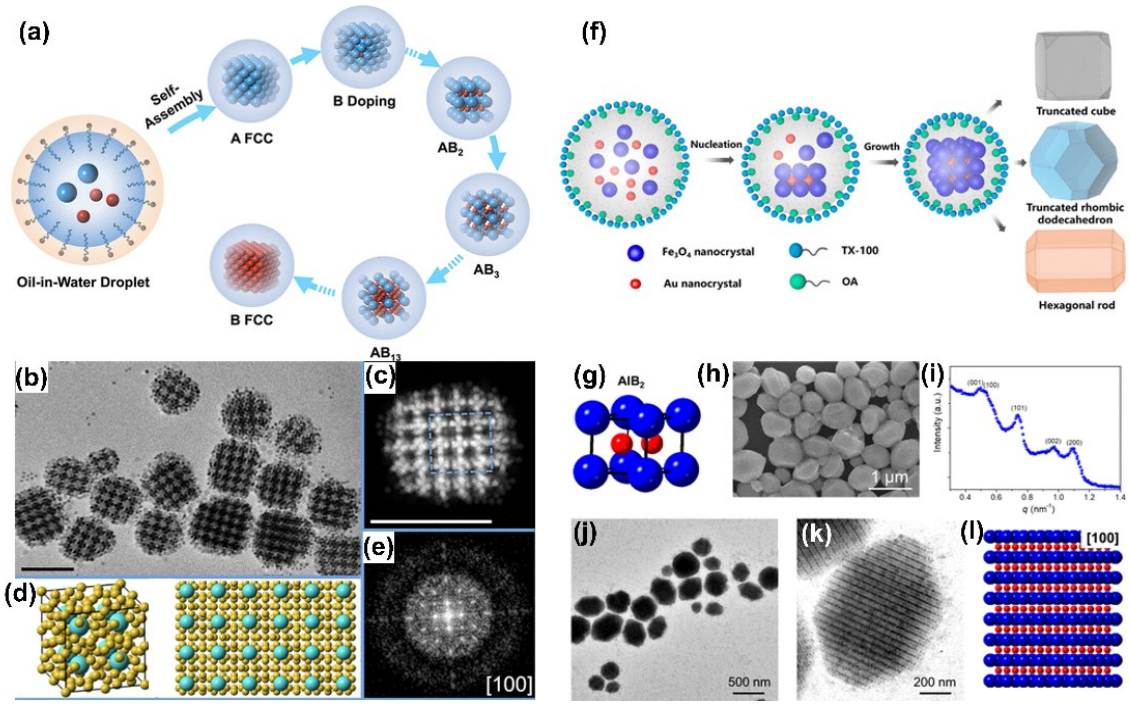

Figure 5. **Binary supercrystals with tunable structural lattices.** (a) Schematic illustration of the formation of colloidal binary supercrystals consisting of two distinct nanoparticle building blocks with different lattice structures by controlling the concentration ratio of two building blocks. (b-e) Characterization of ico-$NaZn_{13}$-type supercrystals. (b) Typical low magnification-TEM image of supercrystals. Scale bar: 100 nm. (c) Typical HAADF-STEM image of an individual supercrystal. Scale bar: 100 nm. (d) The unit cell and [100] projection of the ico-$NaZn_{13}$-type lattice. The yellow and cyan spheres represent Au and Fe_3O_4 nanoparticles, respectively. (e) FFT pattern of the image in (c).[56] **Self-assembly of faceted binary supercrystals.** (f) Schematic illustration of self-assembly of faceted binary nanocrystal supercrystals within emulsion droplets. (g) The unit cell of AlB_2-type crystal. (h) SEM, (i) SAXS profile, (j) TEM, and (k) HAADF-STEM image of AlB_2-type binary supercrystals. (l) Corresponding nanoparticle ordering model in panel k.[65]

It is worth noting that binary superstructures growing by the emulsion-confined assembly process usually adopt spherical shapes due to the template effect from the curved liquid-liquid interface.[64,67] The attractive interaction between alkyl chains of the surfactants and nanoparticles favors the formation of spherical assembled structures. In 2020, Hao et al. reported a novel strategy to control the shape of binary supercrystals by manipulating the

surface property of the emulsion droplets.[65] Choosing surfactants with a bulky hydrophobic part (Triton X-100) and adding co-surfactant (oleic acid) in the oil phase reduce the interaction between surfactants and nanoparticles, favoring the formation of faceted supercrystals, as shown in Figure 5f. Precise control over the size ratio and concentration ratio of two building blocks, namely, Fe_3O_4 and Au nanocrystals, leads to the formation of AlB_2-type binary supercrystals with spindle-like morphology (Figure 5h-k), bcc-AB_6-type binary supercrystals with truncated rhombic dodecahedral morphology, NaCl-type, and $NaZn_{13}$-type binary supercrystals with truncated cube morphology. The morphology of the supercrystals is determined by the intrinsic lattice structures of large nanoparticles. AlB_2-type supercrystals can be elongated by tuning the concentration ratio of [Au]/[Fe_3O_4], producing rod-like morphology with the largest aspect ratio of around 5.

Surfactant stabilized emulsion-confined assembly is a general and powerful strategy to organize colloidal particles into 3D superstructures. This strategy offers more opportunities to control the shape and crystal structure than micelle-based assembly, producing superstructures with complex morphologies.

Pickering emulsion-based self-assembly

Although surfactant-stabilized emulsions have been widely used in many applications, the large-scale use of surfactants in industry or personal care products is not cost-effective. Some surfactants also bring health problems such as irritation and hemolytic behavior.[1] Colloidal particles are a promising alternative and can serve as emulsion stabilizers to produce Pickering emulsions.[19,78,79] With the development of the synthesis techniques of colloidal particles with tunable surface properties, Pickering emulsions and derivative materials with versatile properties were fabricated and utilized in many applications such as drug delivery,[80,81] controlled release,[82,83] and biphasic catalysis.[1,84-86] Pickering emulsions are excellent templates for fabricating colloidosomes due to the good stability of particles at the oil/water interface and natural void structures of emulsion, avoiding the subsequent removal of templates.[1,20,21] The Pickering emulsion-based assembly of colloidal nanoparticles into colloidosomes is illustrated in Figure 6a. The assembly process involves first emulsifying an O/W phase, with colloidal particles either in the oil or water

phase, then the assembly of colloidal nanoparticles at the O/W interface, and finally, the transformation of the assembled superstructures to a fresh solvent.[21] The particle confinement at the oil/water interface is driven by the reduction in Helmholtz free energy and depends on the surface property and size of the colloidal particles. The energy change (ΔE) for one particle confined at the O/W interface can be described by the following equation: $\Delta E = -\frac{\pi r^2}{\gamma_{\frac{O}{W}}}[\gamma_{\frac{O}{W}} - (\gamma_{\frac{P}{W}} - \gamma_{\frac{P}{O}})]^2$ (1)

where r is the size of the particle, and $\gamma_{\frac{O}{W}}$, $\gamma_{\frac{P}{W}}$, and $\gamma_{\frac{P}{O}}$ are the surface energy of oil/water, particle/water, and particle/oil interface, respectively.[21] In general, particles with a contact angle of 15° < ∖ < 90° can stabilize O/W emulsions, whereas W/O emulsions can be stabilized by particles with a contact angle of 90° < ∖ < 165°.[19]

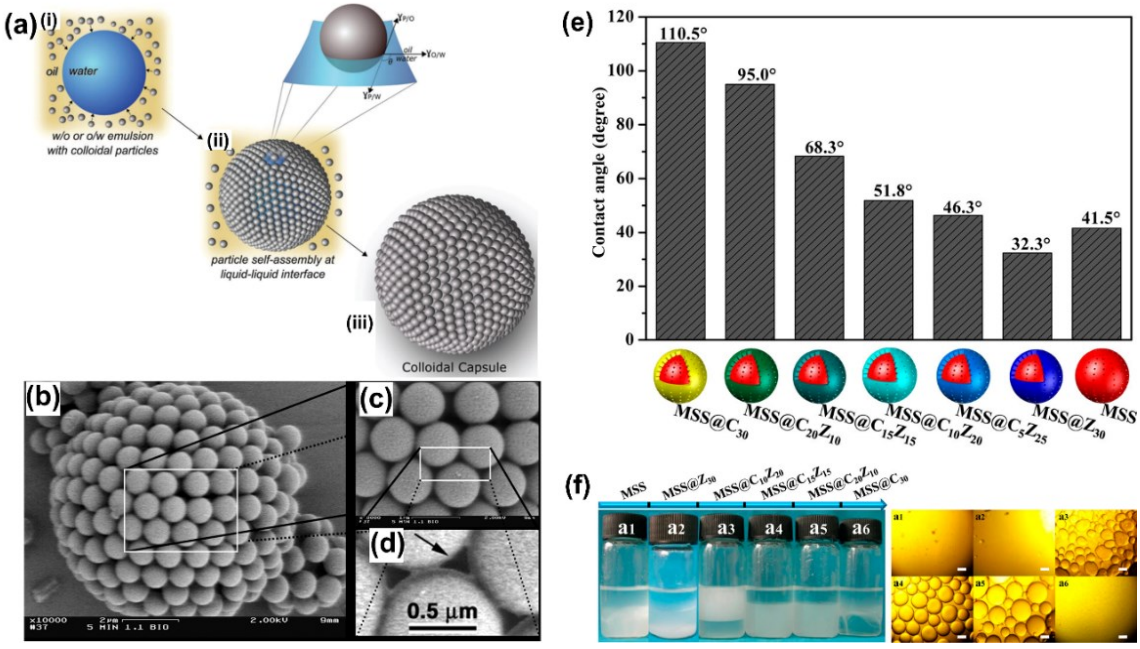

Figure 6. Pickering emulsion-based assembly of hollow superstructures. (a) Schematic illustration of the interfacial assembly of colloidal nanoparticles at the interface of Pickering emulsion.[21] (b-d) Scanning electron microscope image of a dried, 10-μm-diameter colloidosome composed of 0.9-m-diameter polystyrene spheres.[38] (e) Water-solid-air three-phase contact angles of the synthesized mesoporous silica (MSS@C_xZ_y). (f) Appearance (left) and corresponding optical microscopy images (right) of Pickering emulsions stabilized by different mesoporous silicas.[87]

In 2002, Dinsmore et al. reported the first dried colloidosomes from assembling 0.9 μm of polystyrene spheres at the interface of O/W emulsions (as shown in Figure 6b-d). In order to fabricate colloidosomes with precisely tunable permeability, the sample was lightly sintered to bridge the neighboring particle, forming stable elastic shells with uniform holes (Figure 6d).[38] Pickering emulsions can be further stabilized by many methods such as gel trapping,[39] covalent cross-linking,[88] and the polymerization inside or outside emulsion droplets.[89] According to equation 1, the type and stability of Pickering emulsions depend on the surface property of colloidal particles. Xue et al. synthesized mesoporous silica nanoparticles with tunable surface properties, realizing the switching from O/W to W/O Pickering emulsions.[87] Figure 6e shows silica nanospheres incorporated with hydrophilic zwitterionic moiety and hydrophobic octyl moiety in the shell, with the surface property tunable by controlling the ratio of these two functionalities. As shown in Figure 6f, only the silica particles with moderate hydrophilicity or hydrophobicity can stabilize Pickering emulsions. The hydrophilic to hydrophobic switch of silica particle surface property induces the O/W to W/O transit of Pickering emulsion. The concentration of silica particles affects the size of the Pickering emulsion, with more particles leading to smaller droplets (from 1220 to 201 μm). The relationship between these two can be expressed by the following equation:

$$D = \frac{4\rho_p V_d d_p}{m_p} C$$

where m_p is the mass of the emulsifier, D is the size of the emulsion droplet, ρ_p is the density of the emulsifier, V_d is the volume of the dispersed phase, d_p is the average diameter of the emulsifier, and C is the droplet surface coverage. This relationship is consistent with the general understanding that a higher emulsifier concentration allows to stabilize larger droplet interface, thus decreasing the droplet size.

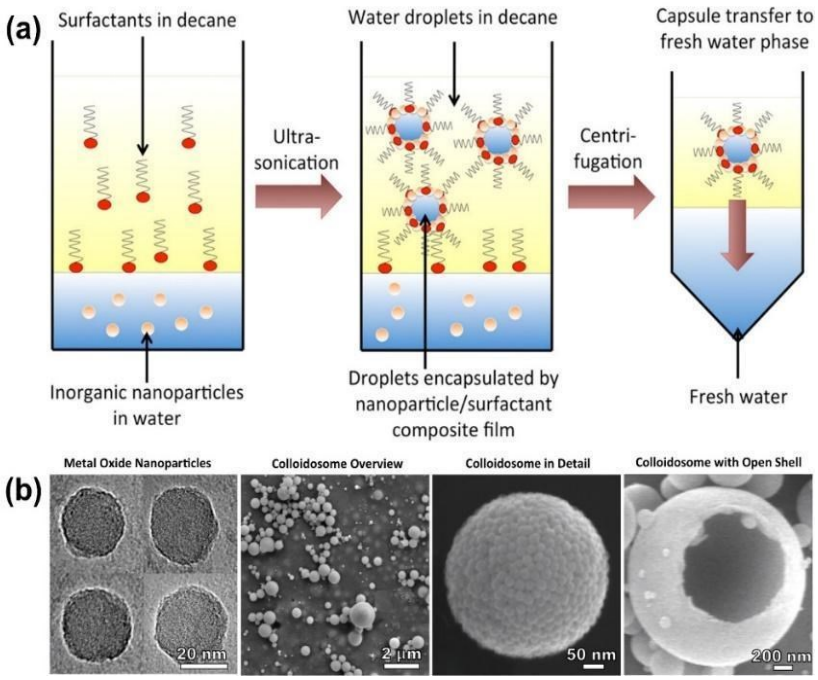

Figure 7. Inverse Pickering emulsion co-stabilized by nanoparticles and surfactants. (a) Schematic illustration of submicron colloidosome preparation. (b) TEM image of SiO_2 nanoparticles, SEM overview image of the colloidosomes, and detailed illustration of representative intact colloidosome as well as colloidosome with a partially open shell.[90]

Micro- or sub-micrometer Pickering emulsions are more attractive for applications in agriculture, the food industry, micro-reactor, catalysis, and drug delivery.[91-94] Although smaller emulsifier particles can produce smaller emulsion droplets, reducing particle sizes decreases ΔE to near k_BT (k_B: Boltzmann constant), allowing easy detachment of particles from the interface.[21] Thus, researchers developed several methods to overcome this problem. For example, Jiang et al. developed a method involving first assembling hydrophobic silica nanoparticles at the inverse W/O emulsion interface and subsequent locking of nanoparticles at the oil-water interface by sol-gel reaction of silica precursor, forming stable sub-micron Pickering emulsions. By controlling the size of silica nanoparticles from 230 nm to 50 nm, they can fabricate colloidosomes with sizes from 1 μm to 200 nm.[95] Since the particle wettability greatly affects the emulsion stability (equation 1), fine-tuning the particle surface property through surfactant modification is an effective way to stabilize Pickering emulsion of submicron sizes. Sihler et al. fabricated stable submicron W/O Pickering emulsions by mixing hydrophilic silica nanoparticles with

poly(ethylene-co-butylene)-block-poly(ethylene oxide). While the pristine silica nanoparticles are too hydrophilic to stay at the W/O interface, the polymer surfactants can adsorb to the silica surface to increase the hydrophobicity and greatly enhance the stability of emulsion droplets.[40] Bollhorst et al. also reported a particle and surfactant co-emulsifier system, and equally charged metal oxides and lipids were used to fabricate W/O Pickering emulsion (as shown in Figure 7).[90] The lipid molecules were attracted to the O/W interface due to the Gibbs adsorption, blocking the interparticle repulsion resulting from the surface charge interaction and driving the agglomeration and controlled self-assembly of the metal oxide nanoparticles at the droplet interface. The same method was used to assemble nanodiamonds[96] and fluorescent and superparamagnetic nanoparticle binary systems[97] into submicron colloidosomes.

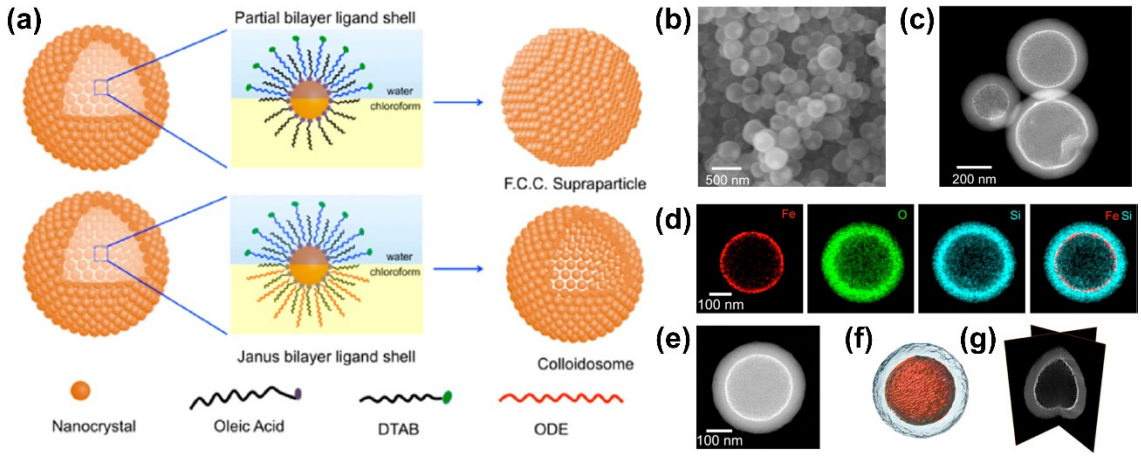

Figure 8. (a) Schematic illustration of the formation mechanism of colloidosomes: a key step is to form the Janus bilayer on the nanocrystal surfaces. (b) SEM image of colloidosomes; (c) HAADF-STEM overview of the colloidosomes; (d) the STEM-EDS maps revealing the distribution of elements; (e) 2D STEM projection from the tomography series; (f) 3D volume rendering of the SIRT tomographic reconstruction; (g) orthogonal slices from panel f.[98]

More complex hollow superstructures were obtained from the Pickering emulsions co-stabilized by nanoparticles and two surfactants, one in the water phase and the other in the oil phase. As shown in Figure 8a, Yang et al. used oleic acid-coated Fe_3O_4 nanoparticles as emulsifier nanoparticles, dodecyltrimethylammonium bromide (DTAB) as an aqueous

surfactant, and octadecene (ODE) as oil phase surfactant to form stable O/W Pickering emulsions.[98] After emulsification, the nanoparticles are adsorbed on the droplet interface driven by the sum of interfacial energy and the van der Waals interaction between the hydrophobic chains of aqueous surfactant and the hydrophobic tails of the surface ligands coated on the nanoparticles. The interaction between ODE and oleic acid modifies the surface of the nanoparticles and contributes to the amphiphilic balance of nanoparticles at the liquid-liquid interface, forming the Janus bilayer ligand shell and favoring the adsorption of nanoparticles at the interface and the formation of a monolayer nanoparticle shell. The nanoparticle shells were stable during solvent evaporation, forming hollow superstructures. In the absence of ODE, spheres of densely packed nanoparticle assemblies were produced. As shown in Figure 8b-e, a layer of silica could be coated on the surface to further stabilize the hollow superstructures. Increasing the concentration of the nanoparticles induced the formation of semi-hollow superstructures with nanoparticle aggregates filling one side of the inner cavity. Further investigation showed that nanoparticles epitaxially grow inside the nanoparticle shells and form densely packed face-centered cubic (*fcc*) supercrystals. Furthermore, when Fe_3O_4 (6.5 ± 0.3 nm) and Au (3.5 ± 0.2 nm) were co-assembled, yolk-shell superstructures with a Fe_3O_4 nanoparticle shell, and a $NaZn_{13}$-type $(FeO_4)Au_{13}$ structure core were formed. Conformal epitaxial growth of superlattice along the nanoparticle shells was forbidden due to the large lattice mismatch between $NaZn_{13}$-type binary supercrystals and the hexagonal structure of the nanoparticle shells.

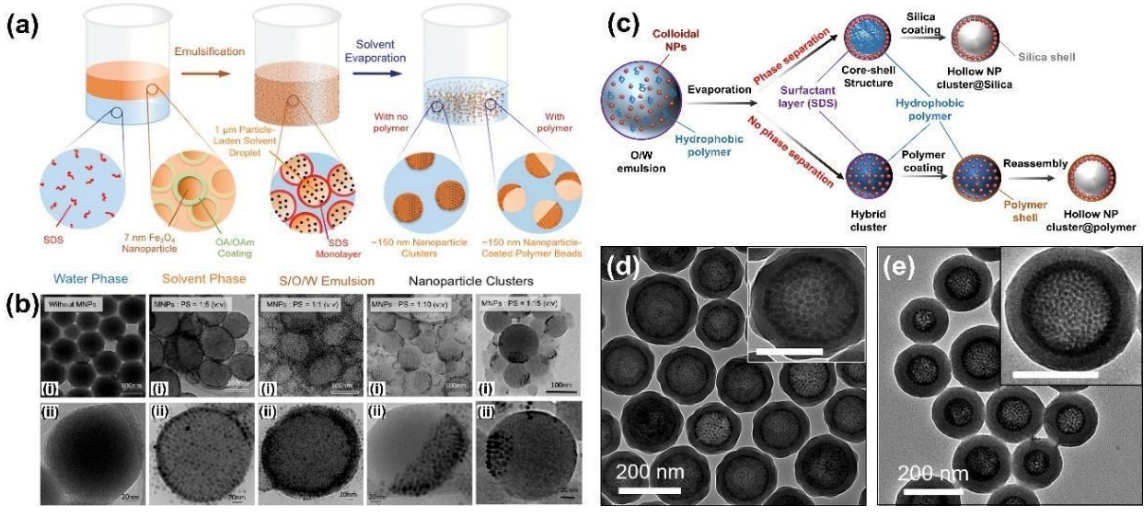

Figure 9. Nanoparticle and surfactant co-stabilized polymer/water inverse Pickering emulsions. (a) Schematic illustration of co-assembly of magnetic nanoparticles and polystyrene within oil/water emulsion droplets to get polymer/magnetic nanoparticle clusters. (b) TEM images of the different assembled structures by controlling the ratio of magnetic nanoparticles and polystyrene.[99] (c) Schematic illustration of the fabrication of hollow superstructures by co-assembling colloidal nanoparticles with either immiscible or miscible polymers within O/W emulsions. TEM images of (d) SiO_2-coated hollow superstructures from the co-assembly of γ-Fe_2O_3 nanoparticles with immiscible polymer: poly(1-decene),[100] (e) RF-coated hollow superstructures from the co-assembly of γ-Fe_2O_3 nanoparticles with miscible polymer: oleic acid oligomers.[61]

In principle, uniform colloidal nanoparticles with sizes ranging from 2-50 nm are ideal candidates to assemble at the O/W interface to form submicron hollow superstructures.[100] However, the detachment of nanoparticles from the interface happens when the particle size is smaller than 50 nm due to thermal fluctuation.[21] According to equation 1, in addition to the surface modification of colloidal nanoparticles through surfactants, increasing the interfacial tension of oil/water and particle/oil is another way to enhance the confinement of nanoparticles at the O/W interface. Isojima et al. developed a general method to fabricate stable submicron polymer/water Pickering emulsions by co-assembling oleic acid-coated Fe_3O_4 (7 nm) nanoparticles with polystyrene within surfactant-stabilized hexane/water emulsions (as shown in Figure 9a).[99] Since polystyrene is incompatible with the oleic acid-coated Fe_3O_4 nanoparticles, the evaporation of hexane induced their phase separation, excluding the nanoparticles from the polymer-rich zone and their assembly at the polymer/water interface. The high interfacial tension of polymer/water and particle/polymer contributes to the stable confinement of nanoparticles at the interface, forming stable polymer/water Pickering emulsions. As shown in Figure 9b, by precisely controlling the polymer/nanoparticle ratio in the oil droplets, monolayer- and multilayer polymer@nanoparticle core-shell structures and partially coated Janus structures were obtained. Recently, our group reported a general method to fabricate submicron hollow superstructures by first co-assembling colloidal nanoparticles with liquid polymers within O/W emulsions and then removing the additive polymers. As shown in Figure 9c, we co-assembled γ-Fe_2O_3 nanoparticles and poly(1-decene) in cyclohexane/water emulsions. The

solvent evaporation induced the phase separation between nanoparticles and polymers and the assembly of nanoparticles at the polymer water interface, producing core-shell structures. The polymer core can be removed by ethanol introduced during the silica coating process, producing stable silica-coated submicron hollow superstructures (Figure 9d).[100] The above two methods utilized the phase separation between nanoparticles and polymers to form colloidosomes. Interestingly, we found that the colloidosomes can also be formed from the co-assembly of nanoparticles and compatible polymers within a shell. As shown in Figure 9c, polymer and nanoparticles were first assembled into hybrid structures and then coated with a layer of resorcinol formaldehyde (RF) shell, followed by the dispersion and reassembly of nanoparticles within the RF shell through penetration and evaporation of the good solvent. The solvent flow and capillary force during evaporation drove the assembly of nanoparticles at the inner surface of the RF shells, producing encapsulated hollow superstructures (Figure 9e).[61] Zhang et al. also reported sub-100 nm colloidosomes from inverse polymer/water Pickering emulsion using polyvinylpyrrolidone (PVP) as both surfactant and oil phase.[101] The addition of dimethylamine induces the formation of PVP/water emulsions by destabilizing the hydrogen bonding between PVP and water, leading to the assembly of ultra-small PVP ligand-capped Au nanoparticles (3.7 nm) at their interfaces. These Au nanoparticles can serve as seeds for the further growth of a second metal, increasing the size of the nanoparticles and further minimizing the Helmholtz free energy for interfacial assembly and increasing the stability of the colloidosomes. Washing with water and acetic acid can remove the PVP templates, forming colloidosomes with a size of sub-100 nm.

In addition to spherical particles, particles with different shapes, like cubes and rods, can also be used as building blocks for assembling colloidosomes. Pang et al. reported a one-step emulsion-based method, which combined the formation and assembly of cubic particles consecutively, producing a monolayer of cubic particle shells whose size can be precisely controlled by the amount of emulsifier.[102] Folter et al. also studied the effect of particle shape anisotropy on Pickering emulsions using cubes and peanuts as building blocks and found that cubes exclusively orient parallel with one of their flat side at the oil-water interface, and peanuts attach parallel with their long side.[103] Noble et al. used

polymeric microrods as building blocks and assembled them at the oil/water interface to produce colloidosomes with a shell of microrods.[104]

Pickering emulsion-based assembly owns its unique advantages from the hollow space of the emulsion droplets, producing colloidosomes with large surface area, abundant active sites, large cavities, and low density. Combining molecular and colloidal particle surfactants enhances the stability greatly and produces colloidosomes with submicron sizes, exploring their practical applications.

Surfactant-free transient emulsion-based self-assembly

Typical assembly of colloidal nanoparticles within or at the interface of emulsion droplets requires good emulsion stability, necessitating many efforts to develop more strategies to improve the stability, such as using surfactants, modifying particle surfaces, and interfacial polymerization. From the application point of view, these additional steps are costly in both materials and processing time and hamper the performance of certain applications like catalysis and electronic devices. For example, surfactants are not only expensive but also block active catalytic sites, lowering the catalytic performance or inhibiting electron transfer.[1,14] Thus, developing an emulsion-based assembly method without extra stabilization steps is highly desirable. In 2015, Liu et al. developed a straightforward method to fabricate plasmonic colloidosomes by assembling gold nanoparticles at the interface of water/1-butanol inverse emulsion.[42] The uniqueness of this emulsion system is the appropriate solubility of water droplets into the 1-butanol continuous phase at their interface, driving the encapsulated nanoparticles toward the interface and assembling them into stable shells. The assembly process is depicted in Figure 10a. It involves the first formation of water/1-butanol emulsion under sonication, then the adsorption of gold nanoparticles at the interface, and finally, the compression of nanoparticle shells upon partial diffusion of interface water into 1-butanol. Further diffusion of water drives the formation of colloidosomes with multilayer nanoparticle shells. As shown in Figure 10b-g, the obtained colloidosomes have a size ranging from 0.5 to 5 μm with multilayer hexagonal close-packed nanoparticle shells. Unlike other inverse Pickering emulsions, the water/1-butanol emulsions serve as transient templates. The partial diffusion drives the

assembly of nanoparticles at the interface, forming stable nanoparticle shells without needing additional surfactants.

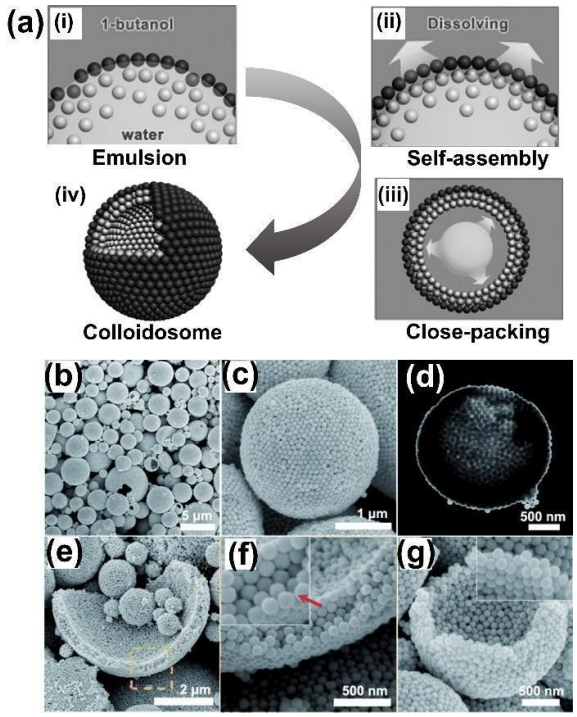

Figure 10. Surfactant-free transient emulsion-based assembly of colloidal nanoparticles into colloidosomes. (a) Self-assembly mechanism of the formation of multilayer colloidosomes. (b, c) SEM images of self-assembled Au colloidosomes, (d) Scanning-TEM image of single Au colloidosome. (e-g) SEM images of the broken Au colloidosomes.[42]

Due to its simplicity and scalability, the emulsion-confined self-assembly of colloidal particles into superstructures is ideal for fabricating metamaterials. However, the intrinsic polydisperse size of emulsion droplets and the difficulty of accurately positioning them limit the control of size, uniformity, and applications of the assembled superstructures. In 2021, we combined the transient emulsion self-assembly strategy with the confinement of well-defined templates patterned on a flat substrate to fabricate superstructures with uniform sizes at all scales.[43] As shown in Figure 11a, a uniform hole pattern is used as a template to encapsulate a water/1-butanol emulsion droplet in each hole, which determines the uniformity and position of the assembled superstructures. The fast diffusion of water into 1-butanol induces the inwards shrinkage of the emulsion droplets and simultaneous

accumulation and self-assembly of colloidal nanoparticles at the water/1-butanol interface, forming colloidosomes with uniform size in each hole. During their shrinkage, the emulsion droplets can well-maintain the quasi-spherical shape tangent to the hydrophobic inner wall of the template, as shown in Figure 11b. The yield reaches near 100%. The size of the colloidosomes can be easily tuned by controlling the nanoparticle concentration or the hole size. Increasing one of them when the other one is fixed increases the size of colloidosomes, producing colloidosomes ranging from 170 nm to 1.43 mm in diameter. Further, the shape of assembled superstructures can be controlled if the building blocks are magnetic nanoparticles. They assemble into 1D chains along the magnetic field direction, forming ellipsoidal colloidosomes with elongated shapes. A stronger magnetic field produced ellipsoids with a larger aspect ratio (Figure 11c). The co-assembly of magnetic and non-magnetic nanoparticles within emulsion droplets under an external magnetic field produces even more complex structures (e.g., tumbler shapes). This strategy is universal for assembling a large variety of building blocks into superstructures, including not only colloidal nanoparticles of different sizes, shapes, and compositions but also biopolymer molecules and ionic compounds.

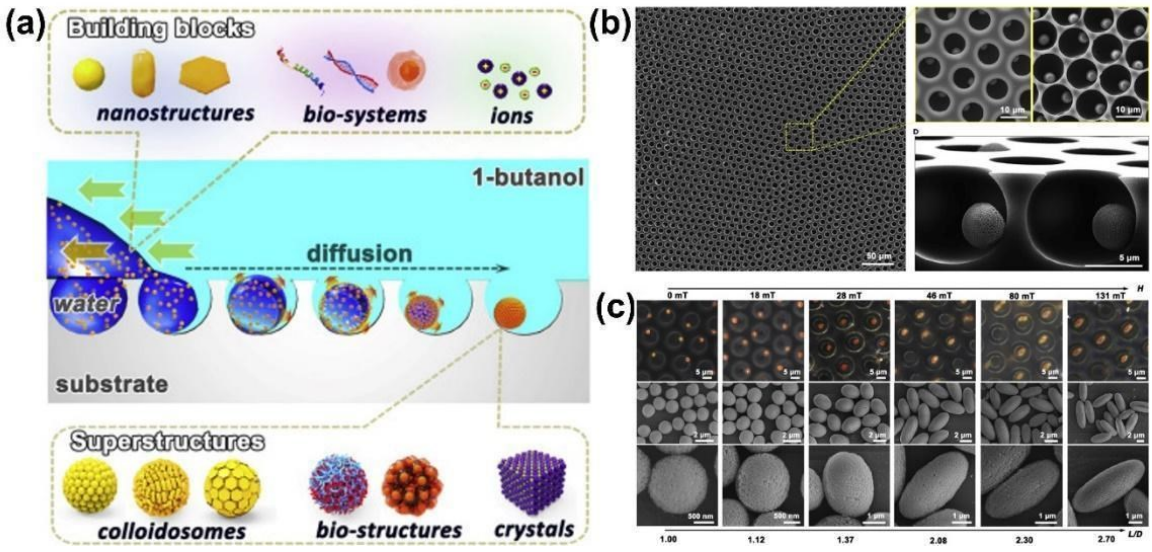

Figure 11. Template-assisted transient emulsion-based assembly of colloidal nanoparticles into colloidosomes. (a) Schematic illustration of the fabrication of colloidosomes based on the template-assisted transient emulsion self-assembly method. (b) SEM images of SiO_2 colloidosomes confined within the template holes. (c) Optical and SEM images of the

shape elongation of assembled Fe_3O_4 colloidosomes by increasing the intensity of the magnetic field.[43]

The new technique based on surfactant-free transient emulsions allows efficient assembly of colloidal nanoparticles into superstructures, featuring cost-effectiveness, environmentally friendliness, and generality. When used in conjunction with well-defined templates, this method offers precise control of the size and position of the assembled superstructures, holding the promise for the fabrication of novel functional devices.

PROPERTIES AND APPLICATIONS

Self-assembly of colloidal nanoparticles within emulsion droplets brings many opportunities to precisely control the size, shape, crystal structure, and component of the assembled superstructures, allowing the exploration of new collective properties (e.g., plasmonic coupling,[101] light absorption,[42] and catalytic activity[105]) and enhanced performances in various applications (e.g., drug delivery,[106] multimodal bioimaging, and therapeutic applications[47,107,108]). These methods typically do not require additional steps for modifying building blocks and can be carried out under mild conditions, making it possible to regulate the particle interaction to generate new synergetic properties while reserving the nanoparticles' intrinsic properties. Co-assembly of functional materials such as plasmonic or fluorescent nanoparticles into superstructures generates interesting optical or catalytic properties such as dual-mode luminescence and plasmon-mediated photocatalyst.[69] Also, the surface property of the assembled structures can be further controlled by coating a layer of a biocompatible shell, for example, silica, for biomedical applications.[47] Furthermore, the hollow space, shell permeability, and reduced transfer resistance of the colloidosomes can be carefully engineered, providing a powerful platform for applications such as catalysis and drug delivery.[20]

Optical properties

Self-assembly of optically active particles into superstructures exhibits enhanced collective properties and unique optical characteristics due to the strong interaction between neighboring particles. Liu et al. reported the fabrication of dark black colloidosomes by

assembling gold nanoparticles within water/1-butanol inverse emulsions (Figure 12).[42] As shown in Figures 12b, c, the original gold nanoparticles show a brick red color, while the assembled colloidosomes appear dark black due to the strong absorption of the incident light in most of the UV/Vis region (Figure 12d), which was caused by the strong plasmonic coupling among the gold nanoparticles within the shells (Figure 12e). Also, the absorption of incident light by the gold colloidosomes was much stronger than planar nanosphere arrays due to the stronger near-field coupling and curved surface of the colloidosomes. Zhang et al. also reported the tunable collective optical properties of the sub-100 nm colloidosomes by assembling gold nanoparticles in PVP/water inverse emulsion.[101] The gold colloidosomes have an overall size of 32 nm. The interparticle nanogaps can be tuned by controlling the seeded growth of gold, showing distinct localized surface plasmon resonance (LSPR) in the visible range of the spectrum. With the decreasing nanogaps from 4.6 to 1.7 nm, the LSPR band shifted towards red from 537 to 578 nm, indicating the convenient tunability for plasmonic applications.

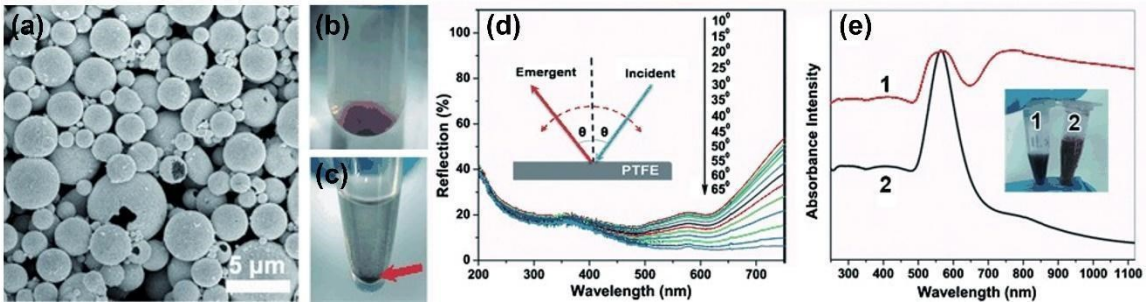

Figure 12. The collective optical property of the gold nanoparticle colloidosomes. (a) SEM image of the self-assembled gold colloidosomes. (b, c) Photo images of the red colloidal gold nanoparticles (b) and black gold colloidosomes settled on the bottom of the tube (c). (d) Reflection spectra of the gold colloidosomes deposited on the PTFE substrate were measured at the angle ranging from 10-65º. (e) The absorption spectra of the black gold colloidosomes (curve 1) and gold nanoparticles (curve 2) dispersed in 1-butanol. The inset in (e) is the corresponding photos of the two solutions.[42]

The co-assembly of two different optically active materials, such as plasmonic and fluorescent nanoparticles, into superstructures brings synergetic optical properties different from their original building blocks. For example, Zhao et al. fabricated binary supercrystals with tunable luminescence properties from the co-assembly of gold and upconversion

($NaYF_4$) nanoparticles within O/W emulsions.[109] With the increase of gold nanoparticles within the superstructures, the upconversion luminescence decreased due to the enhanced Forster resonance energy transfer from the $NaYF_4$ to gold nanoparticles, indicating an easy control of the luminescence properties. Sun et al. also reported bifunctional superparticles fabricated by assembling QDs into superstructures and then overcoating them with a layer of Fe_3O_4 nanoparticles.[110] The assembled superstructures preserve the fluorescent and magnetic properties of the building blocks, showing magnetically responsive fluorescent properties. Hao et al. developed binary supercrystals with faceted morphologies from the co-assembly of Au and Fe_3O_4 nanocrystals within O/W emulsions. The assembled binary supercrystals with different intrinsic lattice structures showed different collective optical properties. The LSPR peak of the assembled structures highly depends on the stoichiometry within supercrystals, and the increasing ratio of Au nanocrystals leads to a larger redshift of the LSPR peak due to the stronger near-field plasmonic coupling.[65]

Catalysis

Nanoparticles have been widely studied as effective catalysts due to their high surface area and abundant active sites. However, nanoparticles, especially metal nanoparticles, tend to reconstruct, diffuse, coalesce, and sinter during the reactions, significantly reducing catalytic properties.[111] Self-assembled superstructures possess intrinsic porous structures, good stability, high surface area, and enhanced catalytic properties, therefore hold promises to overcome this limitation. Xu et al. reported the fabrication of hierarchical colloidosomes with excellent photocatalytic properties by assembling CuO cubic-like particles at the interface of O/W emulsion.[105] The asymmetric Kirkendall effect induced the formation of the open-mouthed hollow structures in the subunit CuO particles, resulting in hierarchical colloidosomes with enhanced light trapping, absorption, and photothermal conversion, and subsequently, a high local temperature (~200 ℃) upon light irradiation. The catalytic CO oxidation reaction rate under light irradiation was 20 times higher than that of thermal catalysis at 240 ℃. Zhang et al. reported sub-100 nm noble metal nanoparticle colloidosomes, which were used as catalysts for the electrochemical formic acid oxidation reaction.[101] Pd colloidosomes, Pd/Au alloys with different atomic ratios colloidosomes, and commercial Pd/Carbon were used as catalysts for the oxidation reaction. The Au-$Pd_{6.5}$

colloidosomes showed the highest mass activity, ~4.3 times that of commercial Pd/Carbon. The nanoparticles within the colloidosomes are closely packed to afford abundant crystallographic defects, effectively reducing the activation energy for the favorable kinetics of the oxidation reaction. Besides, the alloying of Pd with Au brings an additional opportunity to enhance catalytic activity thanks to the bimetallic strain effect.

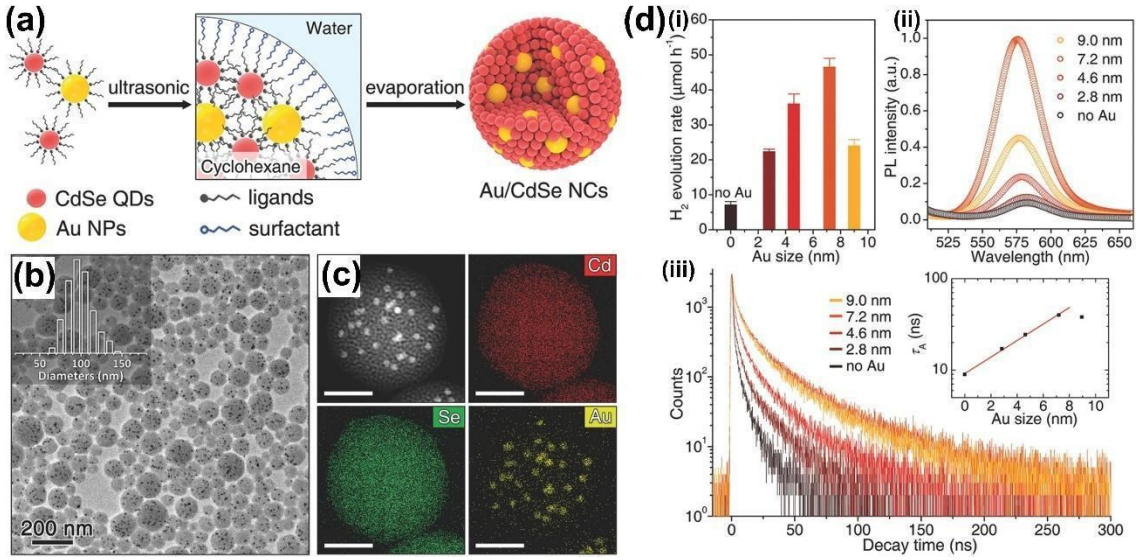

Figure 13. Photocatalytic activity of Binary superstructures. (a) Schematic illustration of the self-assembly of Au and CdSe into binary superstructures within O/W emulsions. (b) TEM, and (c) HAADF-STEM images of Au/CdSe-0.15 superstructures and corresponding EDS maps of Cd, Se, and Au.[69]

Binary superstructures of proper building blocks may exhibit high synergetic catalytic properties. For example, Chen et al. developed a new type of high-temperature catalysts by co-assembling noble metal and oxide nanoparticles within O/W emulsions.[111] The assembled binary superstructures showed excellent thermal stability since the noble-metal nanoparticles are encaged within mesoporous shells composed of oxide nanoparticles, preventing their aggregation and displacement. Thanks to the mesoporosity of the superstructures, the reactant and product molecules can easily reach or exit the surface of the noble-metal nanoparticles. With an overall size below 100 nm, the assembled superstructures maintain a high surface area, further contributing to the high catalytic activity.

Self-assembled superstructures are also the ideal architectures for high-performance electrode materials for lithium-ion batteries.[112,113] In 2018, Yang et al. reported an excellent electrode material from the co-assembly of $CoFe_2O_4$ and Fe_3O_4 nanoparticles into AB_{13}-type binary supercrystals.[67] The average discharge capacity of the binary supercrystals is much higher than that of single-component supercrystals because the local packing arrangement of binary supercrystals greatly affects the electrochemical kinetics. Also, the binary supercrystals can maintain good structural stability during the repeated lithiation and delithiation process, resulting in excellent electrochemical cycling stability.

Plasmon-mediated photocatalysis has recently attracted considerable attention due to the enhanced photoexcitation and improved charge separation in semiconductor photocatalyst systems. Au/CdSe binary superparticles were fabricated, and the synergetic coupling between Au and CdSe was used for the hydrogen evolution reaction (Figure 13).[69] The outstanding extinction cross-section of plasmonic nanoparticles can harvest light and transfer the energy to the neighboring semiconductor through plasmon-induced resonance energy transfer (PRET). The absorption spectrum overlap between Au and CdSe nanoparticles can be precisely controlled by tuning the size of Au nanoparticles and the mass ratio of Au and CdSe nanoparticles to optimize the PRET process. As shown in Figure 13d, all the binary superparticles show higher photocatalytic activity than those without Au. The amount of evolved H_2 increases with Au nanoparticle size from 2.8 to 7.2 nm. Further increasing the particle size to 9 nm leads to a lower catalytic activity due to the severe aggregation, which results in uneven and inefficient energy transfer to the CdSe in the superparticles. Figure 13d (iii) shows time-resolved spectroscopic studies on the photoluminescence decay kinetics. The average lifetime increases with increasing Au nanoparticle size up to 7.2 nm because the light-absorption cross-section and the PRET effect improve with increasing particle size.

Biomedical applications

The self-assembly of colloidal nanoparticles into superstructures with submicron size and tunable properties provides powerful materials for biomedical applications, especially in bioimaging, drug delivery, and therapy.[20] Their collective properties offer excellent

opportunities to greatly enhance biomedical performance and build a multifunctional platform for disease diagnosis and therapy.[47,107] Ortgies et al. reported a multimodal imaging tool for magnetic resonance imaging and infrared fluorescence imaging fabricated from the self-assembly of magnetic iron oxide and QDs nanoparticles within a polymeric matrix.[108] Magneto-fluorescent core-shell superstructures were also developed for in vivo multi-photon and magnetic resonance dual-modal imaging.[47] As shown in Figure 14a, Fe_3O_4 (5.9 ± 0.3 nm) and QDs (9.0 ± 0.4 nm) nanoparticles were co-assembled into core-shell superstructures with a magnetic core and a fluorescent shell. A layer of silica shell was coated on the superstructures to improve biocompatibility and colloidal stability. Thanks to their strong magnetic response, high fluorescence, and small size (~100 nm), the movement of the superstructures within cells could be efficiently manipulated by the magnetic tip. Their trajectories can be accurately tracked (Figure 14b, c). The magneto-fluorescent superstructures can also be used as markers for magnetic resonance imaging (MRI) due to the high degree of aggregation of the core magnetic nanoparticles, giving a high T_2 relaxivity. As shown in Figure 14 d, e, both the magnetic resonance and multi-photon imaging results could reveal the selective accumulation of silica-coated superstructures in the tumor region.

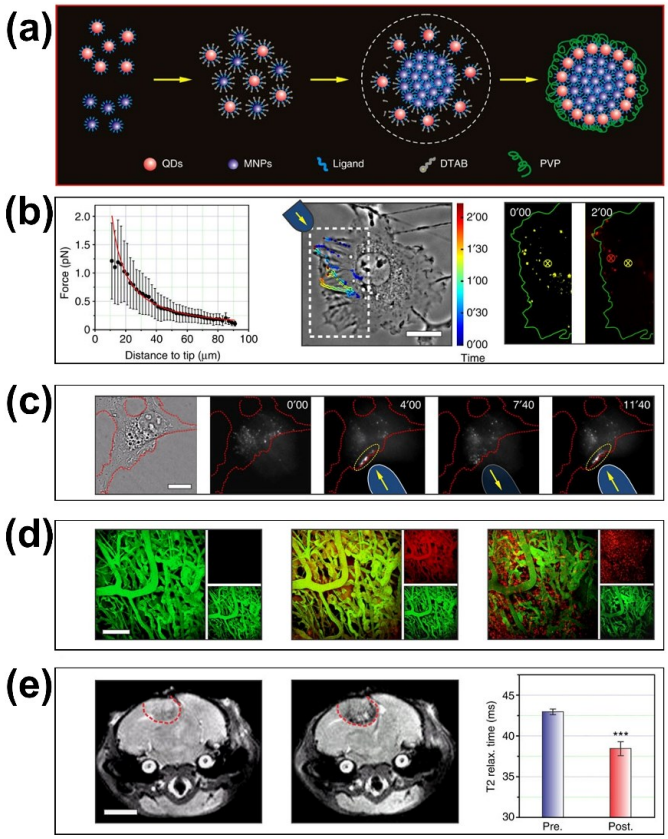

Figure 14. Biomedical applications of the assembled superstructures. (a) Schematic illustration of the formation of core-shell superstructures from the co-assembly of QDs and Fe_3O_4 nanoparticles. (b) Force applied to individual silica-CS-SPs as a function of the distance from the magnetic tip (left), tracking of individual silica-coated superstructures during their manipulation inside a Cos7 cell (middle), fluorescence imaging of individual silica-CS-SPs (yellow) in the dashed line region of middle figure. (c) Transmission picture of a Hela cell in which silica-coated superstructures have been microinjected. (d) Intravital multi-photon microscopy through the cranial window was carried out at different time points: pre-injection (left), 4 h post-injection (middle), and 24 h post-injection (right). Scale bar, 150 μm. (e) In vivo T_2-weighted magnetic resonance images of pre- (left) and 24 h (middle), post-injection of mPEG-silane functionalized silica-coated superstructures.[47]

A multifunctional polymer nanomedical platform for simultaneous cancer-targeted imaging and magnetically guided drug delivery was fabricated from the self-assembly of magnetic or fluorescent nanoparticles with biodegradable poly(D, L-lactic-*co*-glycolic

acid) (PLGA) nanoparticles and doxorubicin (DOXO) (a therapeutic agent for cancers) within O/W emulsions.[107] Cancer-targeting folate was conjugated onto the assembled superstructures by polyethylene glycol groups to target cancer cells, as detected by MRI or confocal microscopy. Furthermore, the magnetic property of the superstructures facilitated the magnetic guiding of the drug delivery, increasing the targeting efficiency. Accordingly, biodegradable Au vesicles allowed more efficient loading of photosensitizers or therapeutic agents.[107] Lin et al. also reported a multifunctional imaging-guided photothermal/photodynamic therapy system based on photosensitizer Ce6-loaded plasmonic gold vesicles.[114] The plasmonic coupling of gold nanoparticles within the vesicles enabled both excitations of gold vesicles and Ce6 to produce heat to kill cancer cells. Also, the heating effect dissociated the vesicles and released the Ce6 molecules, followed by their accumulation in cancer cells, enabling selective destruction of tumor tissues by visualizing through fluorescent, thermal and photoacoustic signals.

CONCLUSION AND OUTLOOK

This review summarizes the current strategies developed for the self-assembly of colloidal particles into 3D superstructures within emulsion droplets. Based on the different stabilizing strategies, the emulsion-confined self-assembly is divided into surfactant-stabilized emulsions, particle-stabilized Pickering emulsions, and surfactant-free transient emulsions. By precisely controlling the surface properties of the colloidal particles and emulsion droplets, one can control the size, shape, and crystal structure of the assembled superstructures. While typically retaining the intrinsic properties of the building blocks, the self-assembly process also creates collective properties by coupling the neighboring particles within the superstructures, offering great opportunities to enhance the catalytic, optical, electric, and magnetic properties. Although significant progress has been made over the years, many challenges still need to be addressed before the emulsion-confined self-assembly methods reach their full potential in practical applications. Below is our view of future directions.

1. Scale up the processes that have the potential to produce superstructures with controllable size and uniformity. Some recent works have demonstrated the feasibility of assembling colloidal particles into uniform superstructures, such as microfluidic device-based and template-assisted assembly.[43,58,115] However, they are limited by the relatively low production yield. It is important to further modify these processes to improve the yield to meet the desired scale of applications.
2. Develop effective means to control the position of the emulsion droplets and the superstructures. Generating superstructures in patterned arrays offers great opportunities for many practical applications as it may allow individual addressability or create collective resonance. However, the intrinsic polydispersity of emulsion droplets adds difficulty to their accurate positioning. The recently demonstrated template-assisted assembly method holds great promise to produce emulsion droplets of uniform sizes nanostructures and deposit them into holes with the desired order.[43] Another possibility is to incorporate active components into the emulsion droplets to facilitate positioning or ordering, for example, under electric or magnetic fields.
3. Explore methods to generate nonspherical superstructures. Limited by the intrinsic shape of droplets, most emulsion-based assembly methods produce spherical superstructures only. Controlling the shape of the superstructures provides another dimension for further manipulating the interaction of coupled nanoparticles with external fields such as light and electric and magnetic fields. To this end, it is critical to explore effective strategies to break the spherical symmetry of the droplets. Magnetic field and nonspherical templates have demonstrated such possibilities, but more should be done to improve the production scale, uniformity, and general applicability to nanostructures of various compositions.
4. Fabricate complex superstructures from more than two types of building blocks with different sizes, shapes, and components. Introducing more particles with different properties brings us more opportunities to explore new collective properties. For example, the formation of 2D ternary superstructures has been explored by assembling different colloidal nanoparticles on a substrate.[116] 3D ternary or even more complex superstructures are expected to show novel

assembled structures, morphologies, and unique properties. For assembly based on Pickering emulsions, most recent studies have focused on unary superstructures. Introducing binary or even more components at the O/W interface is expected to produce hollow superstructures of complex compositions. Fine-tuning the surface property of the nanoparticles may allow control over their spatial distribution within the resulting shells, thereby offering new opportunities to manipulate their catalytic, optical, and other collective properties.

5. Generalize surfactant-free transient emulsion-based assembly methods. While transient emulsion has demonstrated its uniqueness and efficiency in assembling surfactant-free superstructures, the previously developed systems are primarily focused on the water/1-butanol system, limiting the assembly of colloidal particles with surface properties incompatible with these solvents. We expect many new opportunities if this method can be extended to other solvent combinations.
6. Systematically study the physical properties of the assembled structures with different crystal structures, sizes, and components. Thanks to the coupling effect, the superstructures often have different properties than their building blocks in isolated form. More interestingly, their properties highly depend on how the building blocks are arranged relative to each other. Most currently developed methods mainly focus on studying the mechanisms involved in the assembly process. From the applications point of view, it is more interesting to study the effect of crystal structure and morphology of the resulting superstructures on their thermal stability and electric, magnetic, and optical properties.

The emulsion-confined self-assembly is a conceptually simple and general strategy to integrate functional nanoparticles into active superstructures with tunable and collective properties. Continued innovation in manipulating the emulsion droplets and their incorporation with nanoparticles is expected to produce superstructures with precisely controlled size, morphology, composition, structural configuration, and surface property, providing many unconventional materials for building novel functional devices.

Acknowledgements

We are grateful for the financial support from the U.S. National Science Foundation (DMR-1810485).

REFERENCES

1. Jiang, H., Sheng, Y., and Ngai, T. (2020). Pickering emulsions: Versatility of colloidal particles and recent applications. Current opinion in colloid & interface science *49*, 1-15,
2. Tadros, T.F. (2013). Emulsion formation and stability (John Wiley & Sons).
3. Pichot, R. (2012). Stability and characterisation of emulsions in the presence of colloidal particles and surfactants. (University of Birmingham).
4. Nour, A.H. (2018). Emulsion types, stability mechanisms and rheology: A review. International Journal of Innovative Research and Scientific Studies (IJIRSS) *1*,
5. Dziza, K., Santini, E., Liggieri, L., Jarek, E., Krzan, M., Fischer, T., and Ravera, F. (2020). Interfacial properties and emulsification of biocompatible liquid-liquid systems. Coatings *10*, 397,
6. Grossiord, J.L., and Seiler, M. (1999). Multiple emulsions: structure properties and applications (Editions de santé).
7. Walstra, P. (1993). Principles of emulsion formation. Chemical engineering science *48*, 333-349,
8. Wang, Q., Fu, S., and Yu, T. (1994). Emulsion polymerization. Progress in polymer science *19*, 703-753,
9. Chern, C. (2006). Emulsion polymerization mechanisms and kinetics. Progress in polymer science *31*, 443-486,
10. Lovell, P.A., and Schork, F.J. (2020). Fundamentals of emulsion polymerization. Biomacromolecules *21*, 4396-4441,
11. Eliseeva, V.I., Ivanchev, S.S., Kuchanov, S.I.i., and Lebedev, A. (2012). Emulsion polymerization and its applications in industry (Springer Science & Business Media).
12. Abdel-Raouf, M.E.-S. (2012). Factors affecting the stability of crude oil emulsions. Crude oil emulsions–composition, stability and characterization. Croatia: Intech, 183-204,
13. Kale, S.N., and Deore, S.L. (2017). Emulsion micro emulsion and nano emulsion: a review. Systematic Reviews in Pharmacy *8*, 39,
14. Wei, W., Bai, F., and Fan, H. (2019). Surfactant-assisted cooperative self-assembly of nanoparticles into active nanostructures. IScience *11*, 272-293,
15. Boles, M.A., Engel, M., and Talapin, D.V. (2016). Self-assembly of colloidal nanocrystals: From intricate structures to functional materials. Chemical reviews *116*, 11220-11289,
16. Bai, F., Wang, D., Huo, Z., Chen, W., Liu, L., Liang, X., Chen, C., Wang, X., Peng, Q., and Li, Y. (2007). A versatile bottom-up assembly approach to colloidal spheres from nanocrystals. Angewandte Chemie *119*, 6770-6773,
17. Deshmukh, O.S., van den Ende, D., Stuart, M.C., Mugele, F., and Duits, M.H. (2015). Hard and soft colloids at fluid interfaces: Adsorption, interactions, assembly & rheology. Advances in colloid and interface science *222*, 215-227,
18. Yang, Y., Fang, Z., Chen, X., Zhang, W., Xie, Y., Chen, Y., Liu, Z., and Yuan, W. (2017). An overview of Pickering emulsions: solid-particle materials, classification, morphology, and applications. Frontiers in pharmacology *8*, 287,
19. Ortiz, D.G., Pochat-Bohatier, C., Cambedouzou, J., Bechelany, M., and Miele, P. (2020). Current trends in Pickering emulsions: Particle morphology and applications. Engineering *6*, 468-482,

20. Xue, Z., Wang, P., Peng, A., and Wang, T. (2019). Architectural Design of Self-Assembled Hollow Superstructures. Advanced Materials *31*, 1801441,
21. Bollhorst, T., Rezwan, K., and Maas, M. (2017). Colloidal capsules: nano-and microcapsules with colloidal particle shells. Chemical Society Reviews *46*, 2091-2126,
22. Yin, Y., and Alivisatos, A.P. (2005). Colloidal nanocrystal synthesis and the organic–inorganic interface. Nature *437*, 664-670,
23. Yin, S., Li, Z., Cheng, L., Wang, C., Liu, Y., Chen, Q., Gong, H., Guo, L., Li, Y., and Liu, Z. (2013). Magnetic PEGylated Pt 3 Co nanoparticles as a novel MR contrast agent: in vivo MR imaging and long-term toxicity study. Nanoscale *5*, 12464-12473,
24. Ge, J., Hu, Y., Biasini, M., Dong, C., Guo, J., Beyermann, W.P., and Yin, Y. (2007). One-step synthesis of highly water-soluble magnetite colloidal nanocrystals. Chemistry–A European Journal *13*, 7153-7161,
25. Ge, J., Hu, Y., Biasini, M., Beyermann, W.P., and Yin, Y. (2007). Superparamagnetic magnetite colloidal nanocrystal clusters. Angewandte Chemie International Edition *46*, 4342-4345,
26. Gao, A., Xu, W., Ponce de León, Y., Bai, Y., Gong, M., Xie, K., Park, B.H., and Yin, Y. (2017). Controllable Fabrication of Au Nanocups by Confined-Space Thermal Dewetting for OCT Imaging. Advanced Materials *29*, 1701070,
27. Chen, J., Feng, J., Yang, F., Aleisa, R., Zhang, Q., and Yin, Y. (2019). Space-Confined Seeded Growth of Cu Nanorods with Strong Surface Plasmon Resonance for Photothermal Actuation. Angewandte Chemie *131*, 9376-9382,
28. Lu, Z., Gao, C., Zhang, Q., Chi, M., Howe, J.Y., and Yin, Y. (2011). Direct assembly of hydrophobic nanoparticles to multifunctional structures. Nano letters *11*, 3404-3412,
29. Talapin, D.V., Lee, J.-S., Kovalenko, M.V., and Shevchenko, E.V. (2010). Prospects of colloidal nanocrystals for electronic and optoelectronic applications. Chemical reviews *110*, 389-458,
30. Kovalenko, M.V., Manna, L., Cabot, A., Hens, Z., Talapin, D.V., Kagan, C.R., Klimov, V.I., Rogach, A.L., Reiss, P., and Milliron, D.J. (2015). Prospects of nanoscience with nanocrystals. ACS nano *9*, 1012-1057,
31. Li, Z., Wang, W., and Yin, Y. (2020). Colloidal assembly and active tuning of coupled plasmonic nanospheres. Trends in Chemistry *2*, 593-608,
32. Li, Z., Yang, F., and Yin, Y. (2020). Smart materials by nanoscale magnetic assembly. Advanced Functional Materials *30*, 1903467,
33. Li, Z., Fan, Q., Wu, C., Li, Y., Cheng, C., and Yin, Y. (2020). Magnetically tunable plasmon coupling of Au nanoshells enabled by space-free confined growth. Nano letters *20*, 8242-8249,
34. De Nijs, B., Dussi, S., Smallenburg, F., Meeldijk, J.D., Groenendijk, D.J., Filion, L., Imhof, A., Van Blaaderen, A., and Dijkstra, M. (2015). Entropy-driven formation of large icosahedral colloidal clusters by spherical confinement. Nature materials *14*, 56-60,
35. Wang, J., Mbah, C.F., Przybilla, T., Englisch, S., Spiecker, E., Engel, M., and Vogel, N. (2019). Free energy landscape of colloidal clusters in spherical confinement. ACS nano *13*, 9005-9015,
36. Zhuang, J., Wu, H., Yang, Y., and Cao, Y.C. (2007). Supercrystalline colloidal particles from artificial atoms. Journal of the American Chemical Society *129*, 14166-14167,
37. Thompson, K.L., Williams, M., and Armes, S.P. (2015). Colloidosomes: synthesis, properties and applications. Journal of colloid and interface science *447*, 217-228,

38. Dinsmore, A., Hsu, M.F., Nikolaides, M., Marquez, M., Bausch, A., and Weitz, D. (2002). Colloidosomes: selectively permeable capsules composed of colloidal particles. Science *298*, 1006-1009,
39. Duan, H., Wang, D., Sobal, N.S., Giersig, M., Kurth, D.G., and Möhwald, H. (2005). Magnetic colloidosomes derived from nanoparticle interfacial self-assembly. Nano letters *5*, 949-952,
40. Sihler, S., Schrade, A., Cao, Z., and Ziener, U. (2015). Inverse Pickering emulsions with droplet sizes below 500 nm. Langmuir *31*, 10392-10401,
41. Sihler, S., Lindén, M., and Ziener, U. (2017). Highly Transparent w/o Pickering Emulsions without Adjusting the Refractive Index of the Stabilizing Particles. Langmuir *33*, 10302-10310,
42. Liu, D., Zhou, F., Li, C., Zhang, T., Zhang, H., Cai, W., and Li, Y. (2015). Black Gold: Plasmonic Colloidosomes with Broadband Absorption Self-Assembled from Monodispersed Gold Nanospheres by Using a Reverse Emulsion System. Angewandte Chemie International Edition *54*, 9596-9600,
43. Liu, D., Aleisa, R., Cai, Z., Li, Y., and Yin, Y. (2021). Self-assembly of superstructures at all scales. Matter *4*, 927-941,
44. Zhuang, J., Wu, H., Yang, Y., and Cao, Y.C. (2008). Controlling colloidal superparticle growth through solvophobic interactions. Angewandte Chemie International Edition *47*, 2208-2212,
45. Wang, T., Wang, X., LaMontagne, D., Wang, Z., Wang, Z., and Cao, Y.C. (2012). Shape-controlled synthesis of colloidal superparticles from nanocubes. Journal of the American Chemical Society *134*, 18225-18228,
46. Wang, T., Zhuang, J., Lynch, J., Chen, O., Wang, Z., Wang, X., LaMontagne, D., Wu, H., Wang, Z., and Cao, Y.C. (2012). Self-assembled colloidal superparticles from nanorods. Science *338*, 358-363,
47. Chen, O., Riedemann, L., Etoc, F., Herrmann, H., Coppey, M., Barch, M., Farrar, C.T., Zhao, J., Bruns, O.T., and Wei, H. (2014). Magneto-fluorescent core-shell supernanoparticles. Nature communications *5*, 1-8,
48. Wang, T., LaMontagne, D., Lynch, J., Zhuang, J., and Cao, Y.C. (2013). Colloidal superparticles from nanoparticle assembly. Chemical Society Reviews *42*, 2804-2823,
49. Guo, J., Yang, W., and Wang, C. (2013). Magnetic colloidal supraparticles: design, fabrication and biomedical applications. Advanced Materials *25*, 5196-5214,
50. Zhang, Q., Joo, J.-B., Lu, Z., Dahl, M., Oliveira, D.Q., Ye, M., and Yin, Y. (2011). Self-assembly and photocatalysis of mesoporous TiO2 nanocrystal clusters. Nano Research *4*, 103-114,
51. Lu, Z., Ye, M., Li, N., Zhong, W., and Yin, Y. (2010). Self-assembled TiO2 nanocrystal clusters for selective enrichment of intact phosphorylated proteins. Angewandte Chemie International Edition *49*, 1862-1866,
52. Montanarella, F., Geuchies, J.J., Dasgupta, T., Prins, P.T., Van Overbeek, C., Dattani, R., Baesjou, P., Dijkstra, M., Petukhov, A.V., and Van Blaaderen, A. (2018). Crystallization of nanocrystals in spherical confinement probed by in Situ X-ray scattering. Nano letters *18*, 3675-3681,
53. Gu, J., Zhang, W., Su, H., Fan, T., Zhu, S., Liu, Q., and Zhang, D. (2015). Morphology genetic materials templated from natural species. Advanced Materials *27*, 464-478,
54. Song, G., Li, J., Yuan, Y., Yao, L., Gu, J., Liu, Q., Zhang, W., Su, Y., and Zhang, D. (2019). Large-Area 3D Hierarchical Superstructures Assembled from Colloidal Nanoparticles. Small *15*, 1805308,

55. Xu, J., Shang, M., Ni, X., and Cao, Y. (2020). Strategy based on rapid self-assembly of magnetic nanoparticles for construction of photonic crystals. ACS Applied Nano Materials *3*, 8052-8059,
56. Hu, T., Xu, J., Shang, M., Zhao, Q., and Cao, Y. (2022). Photonic crystal sensor for melamine based on magnetic molecularly imprinted nanoparticles self-assembled with an amphiphilic random copolymer. Microchimica Acta *189*, 1-11,
57. Wang, D., Hermes, M., Kotni, R., Wu, Y., Tasios, N., Liu, Y., De Nijs, B., Van Der Wee, E.B., Murray, C.B., and Dijkstra, M. (2018). Interplay between spherical confinement and particle shape on the self-assembly of rounded cubes. Nature communications *9*, 1-10,
58. Wang, J., Mbah, C.F., Przybilla, T., Apeleo Zubiri, B., Spiecker, E., Engel, M., and Vogel, N. (2018). Magic number colloidal clusters as minimum free energy structures. Nature communications *9*, 1-10,
59. Marino, E., Keller, A.W., An, D., Van Dongen, S., Kodger, T.E., MacArthur, K.E., Heggen, M., Kagan, C.R., Murray, C.B., and Schall, P. (2020). Favoring the growth of high-quality, three-dimensional supercrystals of nanocrystals. The Journal of Physical Chemistry C *124*, 11256-11264,
60. Luo, D., Qin, X., Song, Q., Qiao, X., Zhang, Z., Xue, Z., Liu, C., Mo, G., and Wang, T. (2017). Ordered Superparticles with an Enhanced Photoelectric Effect by Sub-Nanometer Interparticle Distance. Advanced Functional Materials *27*, 1701982,
61. Wu, C., Li, Z., Bai, Y., To, D., Myung, N.V., and Yin, Y. (2022). Self-assembly of colloidal nanoparticles into encapsulated hollow superstructures. Aggregate *3*, e146,
62. Park, J.e., Hickey, D.R., Jun, S., Kang, S., Hu, X., Chen, X.J., and Park, S.J. (2016). Surfactant-assisted emulsion self-assembly of nanoparticles into hollow vesicle-like structures and 2D plates. Advanced Functional Materials *26*, 7791-7798,
63. Zhang, X., Han, J., Yao, T., Wu, J., Zhang, H., Zhang, H., Zhang, X., and Yang, B. (2011). Binary superparticles from preformed Fe 3 O 4 and Au nanoparticles. CrystEngComm *13*, 5674-5676,
64. Wang, P.-p., Qiao, Q., Zhu, Y., and Ouyang, M. (2018). Colloidal binary supracrystals with tunable structural lattices. Journal of the American Chemical Society *140*, 9095-9098,
65. Hao, J., Yang, Y., Zhang, F., Yang, Z., and Wei, J. (2020). Faceted colloidal Au/Fe3O4 binary supracrystals dictated by intrinsic lattice structures and their collective optical properties. The Journal of Physical Chemistry C *124*, 14775-14786,
66. Li, P., Peng, Q., and Li, Y. (2009). Dual-mode luminescent colloidal spheres from monodisperse rare-earth fluoride nanocrystals. Advanced Materials *21*, 1945-1948,
67. Yang, Y., Wang, B., Shen, X., Yao, L., Wang, L., Chen, X., Xie, S., Li, T., Hu, J., and Yang, D. (2018). Scalable assembly of crystalline binary nanocrystal superparticles and their enhanced magnetic and electrochemical properties. Journal of the American Chemical Society *140*, 15038-15047,
68. Wang, D., Dasgupta, T., van der Wee, E.B., Zanaga, D., Altantzis, T., Wu, Y., Coli, G.M., Murray, C.B., Bals, S., and Dijkstra, M. (2021). Binary icosahedral clusters of hard spheres in spherical confinement. Nature Physics *17*, 128-134,
69. Shi, R., Cao, Y., Bao, Y., Zhao, Y., Waterhouse, G.I., Fang, Z., Wu, L.Z., Tung, C.H., Yin, Y., and Zhang, T. (2017). Self-assembled Au/CdSe nanocrystal clusters for plasmon-mediated photocatalytic hydrogen evolution. Advanced Materials *29*, 1700803,
70. Kister, T., Mravlak, M., Schilling, T., and Kraus, T. (2016). Pressure-controlled formation of crystalline, Janus, and core–shell supraparticles. Nanoscale *8*, 13377-13384,

71. Gartner, T.E., Heil, C.M., and Jayaraman, A. (2020). Surface composition and ordering of binary nanoparticle mixtures in spherical confinement. Molecular Systems Design & Engineering *5*, 864-875,
72. Shevchenko, E.V., Talapin, D.V., Murray, C.B., and O'Brien, S. (2006). Structural characterization of self-assembled multifunctional binary nanoparticle superlattices. Journal of the American Chemical Society *128*, 3620-3637,
73. Redl, F.X., Cho, K.-S., Murray, C.B., and O'Brien, S. (2003). Three-dimensional binary superlattices of magnetic nanocrystals and semiconductor quantum dots. Nature *423*, 968-971,
74. Shevchenko, E.V., Talapin, D.V., Kotov, N.A., O'Brien, S., and Murray, C.B. (2006). Structural diversity in binary nanoparticle superlattices. Nature *439*, 55-59,
75. Bartlett, P., Ottewill, R., and Pusey, P. (1992). Superlattice formation in binary mixtures of hard-sphere colloids. Physical Review Letters *68*, 3801,
76. Hudson, T., and Harrowell, P. (2008). Dense packings of hard spheres of different sizes based on filling interstices in uniform three-dimensional tilings. The Journal of Physical Chemistry B *112*, 8139-8143,
77. Ben-Simon, A., Eshet, H., and Rabani, E. (2013). On the phase behavior of binary mixtures of nanoparticles. Acs Nano *7*, 978-986,
78. Alkotzer, Y.I., Grzegorzewski, F., Belausov, E., Zelinger, E., and Mechrez, G. (2019). In situ interfacial surface modification of hydrophilic silica nanoparticles by two organosilanes leading to stable Pickering emulsions. RSC advances *9*, 39611-39621,
79. Benhamou, M., and El-Moudny, S. (2017). Review on Pickering emulsions stabilized by adsorbed nanoparticles: Structure, Thermodynamics, Cage Effect and Subdiffusion. International Journal of Nanomaterials, Nanotechnology and Nanomedicine *3*, 057-076,
80. Frelichowska, J., Bolzinger, M.-A., Pelletier, J., Valour, J.-P., and Chevalier, Y. (2009). Topical delivery of lipophilic drugs from o/w Pickering emulsions. International journal of pharmaceutics *371*, 56-63,
81. Tai, Z., Huang, Y., Zhu, Q., Wu, W., Yi, T., Chen, Z., and Lu, Y. (2020). Utility of Pickering emulsions in improved oral drug delivery. Drug Discovery Today *25*, 2038-2045,
82. Dai, L., Li, Y., Kong, F., Liu, K., Si, C., and Ni, Y. (2019). Lignin-based nanoparticles stabilized pickering emulsion for stability improvement and thermal-controlled release of trans-resveratrol. ACS Sustainable Chemistry & Engineering *7*, 13497-13504,
83. Mao, Q., Li, M., Zhang, S., Zhang, X., He, G., and Zhang, W. (2020). Chitosan-hydrophobic alginate nanocomposites stabilized pH-triggered Pickering emulsion for drug controlled-release. International Journal of Biological Macromolecules *162*, 1888-1896,
84. Rodriguez, A.M.B., and Binks, B.P. (2020). Catalysis in Pickering emulsions. Soft Matter *16*, 10221-10243,
85. Zhang, Y., Zhang, M., and Yang, H. (2018). Tuning biphasic catalysis reaction with a pickering emulsion strategy exemplified by selective hydrogenation of benzene. ChemCatChem *10*, 5224-5230,
86. Pera-Titus, M., Leclercq, L., Clacens, J.M., De Campo, F., and Nardello-Rataj, V. (2015). Pickering interfacial catalysis for biphasic systems: from emulsion design to green reactions. Angewandte Chemie International Edition *54*, 2006-2021,
87. Xue, F., Zhang, Y., Zhang, F., Ren, X., and Yang, H. (2017). Tuning the interfacial activity of mesoporous silicas for biphasic interface catalysis reactions. ACS applied materials & interfaces *9*, 8403-8412,

88. Arumugam, P., Patra, D., Samanta, B., Agasti, S.S., Subramani, C., and Rotello, V.M. (2008). Self-assembly and cross-linking of FePt nanoparticles at planar and colloidal liquid− liquid interfaces. Journal of the American Chemical Society *130*, 10046-10047,
89. Schmid, A., Tonnar, J., and Armes, S.P. (2008). A New Highly Efficient Route to Polymer-Silica Colloidal Nanocomposite Particles. Advanced Materials *20*, 3331-3336,
90. Bollhorst, T., Grieb, T., Rosenauer, A., Fuller, G., Maas, M., and Rezwan, K. (2013). Synthesis route for the self-assembly of submicrometer-sized colloidosomes with tailorable nanopores. Chemistry of Materials *25*, 3464-3471,
91. Dickinson, E. (2015). Colloids in food: Ingredients, structure, and stability. Annual review of food science and technology *6*, 211-233,
92. Haag, R. (2004). Supramolecular drug-delivery systems based on polymeric core–shell architectures. Angewandte Chemie International Edition *43*, 278-282,
93. De Koker, S., Hoogenboom, R., and De Geest, B.G. (2012). Polymeric multilayer capsules for drug delivery. Chemical Society Reviews *41*, 2867-2884,
94. Longstreet, A.R., and McQuade, D.T. (2013). Organic reaction systems: using microcapsules and microreactors to perform chemical synthesis. Accounts of Chemical Research *46*, 327-338,
95. Jiang, H., Hong, L., Li, Y., and Ngai, T. (2018). All-Silica Submicrometer Colloidosomes for Cargo Protection and Tunable Release. Angewandte Chemie *130*, 11836-11840,
96. Maas, M., Bollhorst, T., Zare, R.N., and Rezwan, K. (2014). Diamondosomes: Submicron colloidosomes with nanodiamond shells. Particle & Particle Systems Characterization *31*, 1067-1071,
97. Bollhorst, T., Shahabi, S., Wörz, K., Petters, C., Dringen, R., Maas, M., and Rezwan, K. (2015). Bifunctional submicron colloidosomes coassembled from fluorescent and superparamagnetic nanoparticles. Angewandte Chemie *127*, 120-125,
98. Yang, Z., Altantzis, T., Zanaga, D., Bals, S., Tendeloo, G.V., and Pileni, M.-P. (2016). Supracrystalline colloidal eggs: epitaxial growth and freestanding three-dimensional supracrystals in nanoscaled colloidosomes. Journal of the American Chemical Society *138*, 3493-3500,
99. Isojima, T., Suh, S.K., Vander Sande, J.B., and Hatton, T.A. (2009). Controlled assembly of nanoparticle structures: spherical and toroidal superlattices and nanoparticle-coated polymeric beads. Langmuir *25*, 8292-8298,
100. Wu, C., Lu, Z., Li, Z., and Yin, Y. (2021). Assembly of Colloidal Nanoparticles into Hollow Superstructures by Controlling Phase Separation in Emulsion Droplets. Small Structures *2*, 2100005,
101. Zhang, L., Fan, Q., Sha, X., Zhong, P., Zhang, J., Yin, Y., and Gao, C. (2017). Self-assembly of noble metal nanoparticles into sub-100 nm colloidosomes with collective optical and catalytic properties. Chemical science *8*, 6103-6110,
102. Pang, M., Cairns, A.J., Liu, Y., Belmabkhout, Y., Zeng, H.C., and Eddaoudi, M. (2013). Synthesis and integration of Fe-soc-MOF cubes into colloidosomes via a single-step emulsion-based approach. Journal of the American Chemical Society *135*, 10234-10237,
103. de Folter, J.W., Hutter, E.M., Castillo, S.I., Klop, K.E., Philipse, A.P., and Kegel, W.K. (2014). Particle shape anisotropy in Pickering emulsions: cubes and peanuts. Langmuir *30*, 955-964,
104. Noble, P.F., Cayre, O.J., Alargova, R.G., Velev, O.D., and Paunov, V.N. (2004). Fabrication of “hairy” colloidosomes with shells of polymeric microrods. Journal of the American Chemical Society *126*, 8092-8093,

105. Xu, J., Li, X., Wu, X., Wang, W., Fan, R., Liu, X., and Xu, H. (2016). Hierarchical CuO colloidosomes and their structure enhanced photothermal catalytic activity. The Journal of Physical Chemistry C *120*, 12666-12672,
106. Song, J., Yang, X., Yang, Z., Lin, L., Liu, Y., Zhou, Z., Shen, Z., Yu, G., Dai, Y., and Jacobson, O. (2017). Rational design of branched nanoporous gold nanoshells with enhanced physico-optical properties for optical imaging and cancer therapy. ACS nano *11*, 6102-6113,
107. Kim, J., Lee, J.E., Lee, S.H., Yu, J.H., Lee, J.H., Park, T.G., and Hyeon, T. (2008). Designed fabrication of a multifunctional polymer nanomedical platform for simultaneous cancer-targeted imaging and magnetically guided drug delivery. Advanced Materials *20*, 478-483,
108. Ortgies, D.H., De La Cueva, L., Del Rosal, B., Sanz-Rodríguez, F., Fernandez, N., Iglesias-De La Cruz, M.C., Salas, G., Cabrera, D., Teran, F.J., and Jaque, D. (2016). In vivo deep tissue fluorescence and magnetic imaging employing hybrid nanostructures. ACS Applied Materials & Interfaces *8*, 1406-1414,
109. Zhao, J., Wu, J., Xue, J., Zhu, Q., and Ni, W. (2016). Au/NaYF4: Yb, Er binary superparticles: synthesis and optical properties. Israel Journal of Chemistry *56*, 242-248,
110. Sun, X., Ding, K., Hou, Y., Gao, Z., Yang, W., Jing, L., and Gao, M. (2013). Bifunctional superparticles achieved by assembling fluorescent CuInS2@ ZnS quantum dots and amphibious Fe3O4 nanocrystals. The Journal of Physical Chemistry C *117*, 21014-21020,
111. Chen, C., Nan, C., Wang, D., Su, Q., Duan, H., Liu, X., Zhang, L., Chu, D., Song, W., and Peng, Q. (2011). Mesoporous Multicomponent Nanocomposite Colloidal Spheres: Ideal High-Temperature Stable Model Catalysts. Angewandte Chemie *123*, 3809-3813,
112. Guo, G., Ji, L., Shen, X., Wang, B., Li, H., Hu, J., Yang, D., and Dong, A. (2016). Self-assembly of transition-metal-oxide nanoparticle supraparticles with designed architectures and their enhanced lithium storage properties. Journal of Materials Chemistry A *4*, 16128-16135,
113. Lee, S.H., Yu, S.-H., Lee, J.E., Jin, A., Lee, D.J., Lee, N., Jo, H., Shin, K., Ahn, T.-Y., and Kim, Y.-W. (2013). Self-assembled Fe3O4 nanoparticle clusters as high-performance anodes for lithium ion batteries via geometric confinement. Nano letters *13*, 4249-4256,
114. Lin, J., Wang, S., Huang, P., Wang, Z., Chen, S., Niu, G., Li, W., He, J., Cui, D., and Lu, G. (2013). Photosensitizer-loaded gold vesicles with strong plasmonic coupling effect for imaging-guided photothermal/photodynamic therapy. ACS nano *7*, 5320-5329,
115. Wang, L., and Wang, J. (2019). Self-assembly of colloids based on microfluidics. Nanoscale *11*, 16708-16722,
116. Paik, T., Diroll, B.T., Kagan, C.R., and Murray, C.B. (2015). Binary and ternary superlattices self-assembled from colloidal nanodisks and nanorods. Journal of the American Chemical Society *137*, 6662-6669,